A Theoretical Analysis of the Proton and Hydride Transfer in Liver Alcohol Dehydrogenase (LADH)

Qiang Cui,[†] Marcus Elstner,[‡,§] and Martin Karplus*[,†,||]

Departments of Chemistry and Chemical Biology and of Physics, Harvard University, Cambridge, Massachusetts 02138, Department of Theoretical Physics, University of Paderborn, D-33098 Paderborn, Germany, and Laboratoire de Chimie Biophysique, ISIS, Université Louis Pasteur, 67000 Strasbourg, France

Received: August 2, 2001; In Final Form: November 26, 2001

The proton and hydride transfers in horse liver alcohol dehydrogenase (LADH) were studied with a potential surface obtained by use of the self-consistent-charge−density-functional-tight-binding (SCC−DFTB) QM/MM method implemented in the CHARMM program; a correction for solvent shielding was introduced by use of a continuum model. The proton transfers were found to proceed in a virtually concerted fashion before the hydride transfer. The calculations also showed that a radical mechanism, suggested as a possibility in the literature for the H transfer between the substrate and NAD^+, is very unlikely. The energetics of the reaction and pK_a's of residues involved in catalysis indicate that the chemical steps of LADH, as characterized by the calculated value of k_{cat}, are slow for a pH below 5.5, and the hydride transfer is hardly affected for pH between 5.5 and 8.1. These results are compared with the experimentally measured pH dependence of k_{cat} for LADH, although a quantitative comparison is difficult because the chemical steps are only partially rate-limiting in the experiments. A perturbation analysis of the QM/MM energies suggest that a number of charged residues close to the active site (i.e., Asp 49, Glu 68, and Arg 369), as well as the phosphate groups of NAD^+, make important contributions to the energetics of the proton and hydride transfer reactions; mutation experiments to test these predictions would be of interest. Ser 48 interacts with the substrate via a short hydrogen bond, which leads to an inverse solvent isotope effect, in accord with experiment. The overall calculated barrier and endothermicity and the effect of the double mutation (F93W,V203A) on the hydride transfer are in qualitative agreement with measurements; i.e., the hydride transfer barrier is higher in the mutant, presumably due mainly to the fact that the average distance between the donor and acceptor is larger. In accord with the study of Alhambra et al. (Alhambra, C.; Corchado, J. C.; Sánchez, M. L.; Gao, J.; Truhlar, D. G. *J. Am. Chem. Soc.* **2000**, *122*, 8197.), hydride tunneling was shown to be very important for the calculated magnitude of kinetic isotope effects and the Swain−Schaad exponents, although the absolute contribution of tunneling to the rate constant is calculated to be small (a factor of 2) at room temperature. It was shown that the secondary Swain−Schaad exponent can be affected by the variation in the position of the transition state upon secondary isotopic substitution. The exponent, therefore, does not necessarily reflect the magnitude of tunneling; i.e., one has to be cautious in using the secondary Swain−Schaad exponent to estimate the magnitude of tunneling. Equilibrium effects of protein "dynamics" on the hydride transfer in LADH were studied by potential of mean force calculations at different temperatures. To obtain a clearer description of the origin of the calculated variation, an analysis was made with the QM and MM atoms maintained at different temperatures by use of Nosé−Hoover thermostats. It was found that the barrier is correlated primarily with the temperature of the QM region, while the temperature of the MM atoms has a larger effect on the exothermicity. The variation of the barrier with the structures accessible by molecular dynamics simulations was found to be small (<1 kcal/mol). The effect arises mainly from the change in the position of residues that directly interact with the reacting groups, such as Ser 48.

I. Introduction

Enzyme catalyzed reactions have been studied experimentally and theoretically for many years to determine the origin of the observed rate increase, which can be as large as 17 orders of magnitude.[1] Recently, attention has focused on dynamical effects and tunneling, particularly for hydrogen transfer, and it has been suggested that they may play a significant role in the observed rate enhancement. An enthusiastic description of such studies is given by E. K. Wilson in *Chem. Eng. News*;[2] see, also, the discussion of Sutcliffe and co-workers.[3] Because of the many structural and kinetic studies of alcohol dehydrogenases (ADH), these enzymes, which catalyze hydride transfer reactions, have become model systems for the analysis of such effects.[4] Of particular importance in this regard is the work of Klinman and co-workers that has used kinetic isotope effects (KIE) and the temperature dependence of the reaction in mesophilic and thermophilic ADH to study the role of dynamics and tunneling.[5]

Alcohol dehydrogenase (ADH) is a dimeric enzyme that catalyzes the oxidation of alcohols to aldehydes (or to carboxylic

[†] Department of Chemistry and Chemical Biology.
[‡] Department of Physics.
[§] Department of Theoretical Physics.
[||] Laboratoire de Chimie Biophysique.

10.1021/jp013012v CCC: $22.00
Published on Web 02/16/2002

SCHEME 1

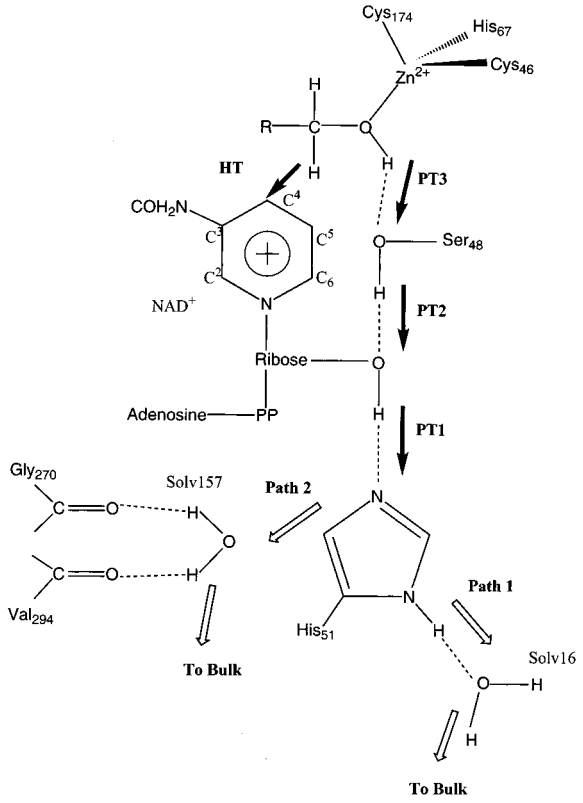

acids by a dismutation). The reaction is stereospecific and belongs to the class A of the dehydrogenase family.[1] A large number of X-ray[6,7] and kinetic[8,9] studies have been made to investigate the catalytic mechanism. It is generally accepted that a hydrogen is transferred as a hydride from the hydroxylic carbon of the alcohol substrate to position 4 of the cofactor, nicotinamide adenine dinucleotide (NAD^+), although a radical mechanism has not been ruled out experimentally.[1,4] A second hydrogen from the hydroxyl group of the alcohol is released as a proton to the solvent. One of the active-site zinc ion is believed to facilitate the hydride transfer from the alcohol to the NAD^+;[6] the other zinc ion is believed to play a structural role. From kinetic studies at different pH,[10] it was proposed that the hydride transfer is preceded by deprotonation of the zinc-bound alcohol.[11] A suggested pathway for the proton transfer from the alcohol to solvent proceeds through a hydrogen-bonded network[6] consisting of the hydroxyl group of Ser 48, the 2′-hydroxyl group of NAD^+ and His 51 (see Scheme 1).[12,13] For the initial hydride transfer step, both primary and secondary substrate KIE values have been measured, and the results were interpreted as evidence for hydride tunneling.[5,14,15] Although no deuterium solvent isotope effect was observed in an early study,[16] more recent work has found an inverse deuterium solvent isotope effect for horse liver alcohol dehydrogenase with ethanol[17] and benzyl alcohol[9] as the substrate. The result was interpreted as due to the presence of a strong hydrogen bond between the negatively charged oxygen atom in the substrate and the hydroxyl group in Ser 48, with the assumption that the motion of the hydroxyl proton of Ser 48 was significantly coupled to the hydride transfer. This leads to a solvent isotope effect if the alcohol or Ser 48 can exchange a proton with the solvent.[9] The rate-limiting step in ADH varies for different species; it is the chemical step in yeast with benzyl alcohol as the substrate.[4,18] After the hydride transfer, NADH also has to dissociate and get replaced by NAD^+; in LADH, the dissociation of NADH is the rate-limiting step. For example, the dissociation constants for the benzyl aldehyde and NADH in LADH are 79 and 6.3 s^{-1}, respectively; for comparison, the rate for the chemical step is measured to be 47 s^{-1}.[8] The fact that the chemical steps are not fully rate-limiting in LADH (i.e., the presence of "kinetic complexity") has made difficult the interpretation of experimental isotope effects[5,14,15] (such as the contribution due to hydride tunneling). Thus, it is useful to analyze the chemical steps directly (which can be readily done with computational approaches) to better understand the kinetics of LADH and to identify the residues that play important roles in the chemical catalysis.

A number of theoretical studies of the mechanisms of LADH and the contribution of tunneling in the hydride transfer have been published recently.[19−21] In this paper, we focus on three aspects of the enzyme catalyzed reaction by LADH with ethyl alcohol as the substrate. The first concerns the question of whether the proton transfer along the proposed hydrogen-bonded network is stepwise or concerted. In a recent theoretical analysis a stepwise mechanism was proposed.[20] However, we find that the reaction is essentially concerted. Understanding this aspect of the hydride/proton transfer is of great interest because proton release from a protein to the bulk solvent (and the reverse process of proton uptake from the bulk solvent by a protein) is an important reaction that takes place in many biologically relevant processes.[22] Examples are proton transfers in bioenergetic phenomena involving systems such as bacteriorhodopsin,[23] the photosynthetic reaction,[24] and ATP synthase.[25] The second aspect concerns the role of tunneling in the LADH reaction. After this work was essentially completed, a theoretical paper with a careful analysis of the problem and a calculation of tunneling effects was published by Alhambra et al.;[21] it supplements the more phenomenological analysis of tunneling in LADH by Rucher and Klinman.[26] In the present paper, a treatment of tunneling similar to that in ref 21 is employed, but a larger number of atoms are allowed to move in the tunneling calculations (278 vs 21 in ref 21); the temperature dependence of the hydride transfer rate constant and the contribution due to tunneling are also examined briefly. In addition, a different method is used for determining the potential surface for the reaction. Finally, we investigate briefly the effect of structural fluctuations on the hydride transfer; i.e., we examine whether there is a connection between the flexibility of the enzyme and catalysis in LADH. As mentioned above, experiments have been *interpreted* as providing evidence for the important role of "dynamics" in catalysis. This includes the kinetic studies on a number of alcohol dehydrogenases from different species over a range of temperatures,[5,14,15] glucose oxidase with different degrees of glycosylation,[5a,27] and the pressure dependence of isotope effects found in yeast alcohol dehydrogenase.[18] However, there is little direct information on the precise nature of the "dynamics" implicated in these systems. Model studies have suggested, in agreement with earlier analyses, that the vibrations of the proton/hydride donor and acceptor are likely to be involved.[28,29] We explore the roles of flexibility and dynamics in determining the activation barrier and tunneling, which have not been analyzed in previous theoretical studies.

One of the difficulties in extending methods that have been applied to small molecule reactions to enzymes is that the latter are not "small" by any criterion. Consequently, rather approximate methods have to be used for determining the potential energy or potential-of-mean-force (PMF) surface for the reaction and for the dynamics on that surface. Because of the sensitivity

of the tunneling contribution to the details of the surface (particularly the width of the barrier), the choice of the quantum mechanical method for determining the surface plays a crucial role in the results. This contrasts with the analysis of the contributions of the enzyme to the lowering of the barrier, which can be understood with more approximate quantum mechanical methods because the quantitative results are often of less interest than the qualitative understanding of the catalytic effects. In some cases (e.g., to distinguish a concerted from a stepwise mechanism), the accuracy of the surface is more important. The study of the mechanism cited above[20a] used the PM3 semiempirical method for the analysis, while the tunneling calculation[21] for the hydride transfer step used a simplified LEPS-type equation,[30] which is essentially as fast to calculate as the MM terms; their use of the LEPS formula is analogous to a prior calculation of the transmission coefficient by activated dynamics in triosephosphate isomerase.[31]

We have recently implemented[32] a DFT-based semiempirical method, the SCC−DFTB approach,[33] in the CHARMM program[34] for the purpose of doing QM/MM studies[35] of complex systems, such as enzymes. The SCC−DFTB potential has been demonstrated to be more accurate than the commonly used AM1 and PM3 algorithms,[32] particularly for system involving proton transfers and metal ions.[36] It appears worthwhile, therefore, to reinvestigate both the nature of the mechanism and the tunneling contribution to the LADH reaction with the SCC−DFTB/MM method,[32] which provides a computational approach that is both fast and sufficiently accurate for examining the problem at hand. Moreover, studying the same system with different approaches is important for assessing the reliability of the methodology. We have chosen to consider ethyl alcohol as the substrate, in contrast to refs 20 and 21, which used benzyl alcohol. This is because the X-ray structure of LADH with DMSO as the ligand[37] (it is thought to be a product (aldehyde) analogue) has a higher resolution (1.8 Å) compared to that for benzyl alcohol with fluoro/bromo-benzyl alcohol as the inhibitor (2.1 Å).[7] Furthermore, a mutant structure of LADH used in the current work was determined with trifluoroethanol as the inhibitor.[15] Previous studies suggest that the mechanism and kinetics for ethyl and benzyl alcohol are similar.[9,17] For example, the turnover numbers in the forward and reverse direction are 3.5 and 47 s^{-1} for ethanol and the corresponding values for benzyl alcohol are 3.1 and 110 s^{-1}.[9] The Michaelis constant for ethanol, however, is substantially larger than that for benzyl alcohol; it is 0.35 mM for the former and 0.028 mM for the latter.[9] Comparison of the X-ray structures with different ligands (PDB code 2OHX with DMSO and 1HLD with 2,3,4,5,6-pentafluorobenzyl alcohol) show that the active site structures are essentially the same. Moreover, the similarity in the computed barrier for the hydride transfer obtained from reaction path and potential of mean force calculations (see text), indicates that the orientation of the substrate (modeled on the basis of the DMSO structure) is satisfactory and that small changes in position do not have an important effect. Although the choice of substrate in this work and previous theoretical studies can have some effect on the quantitative results, the major differences are likely to be due to the computational methods, particularly the potential energy function employed. Many aspects of the reaction, such as the temperature dependence of the kinetic isotope effects and the effect of enzyme flexibility on the chemical step, which are the major focuses of the current work, are not expected to depend strongly on the substrate. However, the difference in the substrates must be kept in mind when quantitative differences between the calculations are considered.

II. Method

The potential surface calculations were performed with the QM/MM methodology, using SCC−DFTB for the QM part and the CHARMM22 force field for the MM part.[38] For the geometry optimization, the SCC−DFTB region consists of 79 atoms that are involved in the proton/hydride transfer network; these are the substrate, the nicotinamide and the ribose of NAD^+, the Zn ion plus its three amino acid ligands (Cys 46 and 174 and His 67), Ser 48, and His 51 (see Figure 1). The later two were included in the QM region because they are believed to be involved in the proton transfer from the alcohol to the bulk solvent. The proton transfer from His 51 to the bulk was not modeled explicitly, and therefore the water molecules close to His 51, and Solv 16 and 157, were not included in the QM region. Due to the rather diffuse electron distribution for the hydride during the reaction, the SCC−DFTB parameters for C and H were reparametrized (see Supporting Information): this corresponds to the use of a more diffuse basis function in ab initio or DFT calculations.[39] It should be emphasized, however, that no LADH related models were included in the reparametrization and therefore the new parameters should be valid for hydride transfer reaction in general. For the interactions between the QM and MM regions within a molecule (e.g., an amino acid side chain and the rest of the protein), the link atom method[35] was used to saturate the valence of the QM boundary atoms. The link atoms interact through electrostatic interaction with all the MM atoms except for the MM boundary atom (the so-called link host). Previous test calculations suggest that such a scheme is a reliable way to treat the QM/MM boundary problem, particularly when the MM atoms in the region of the link atoms have small charges,[40] as they do here; i.e., the C_α atoms in the amino acids have charge of +0.07 and the link hosts in NAD^+ have partial charges of +0.14. A stochastic boundary[41] treatment with a 25 Å radius sphere centered on the alcohol oxygen in the substrate was used for the active site of one of the subunits (33 residues from the other subunit were included) and Poisson−Boltzmann charge scaling[42] was introduced to account for solvent shielding not included via the explicit water molecules[43] in the model. A few charged residues that are spatially close to the QM region and buried in the enzyme were not scaled: they are Asp 49, Glu 68, and Arg 369; the partial charges on the NAD^+ group were also not scaled. A dielectric constant of 4 for the protein and 80 for the solvent was employed in the Poisson−Boltzmann calculations; the former value has been found to be appropriate in comparison with free energy calculations of ligand binding.[44] The final model includes 5400 protein atoms, 186 X-ray water molecules, and 553 additional water molecules required to complete the stochastic boundary sphere (see Figure 1).

As the starting structure, the X-ray structure (1.8 Å resolution)[37] of the horse LADH−NADH complex with the product analogue DMSO was chosen. The DMSO was transformed to ethyl alcohol by replacing the sulfur atom with C and deleting one carbon atom pointing away from the NAD^+. After minimization with 500 steps of steepest descent followed by 1500 steps of adapted basis Newton−Raphson[34] using QM/MM, the rms difference from the X-ray structure in the active region of the stochastic boundary system was 0.40 Å (0.56 Å) for the mainchain (all heavy atoms). Exploratory calculations were made also for a double mutant, F93W,V203A that has been studied experimentally;[15] the 2 Å X-ray structure determined

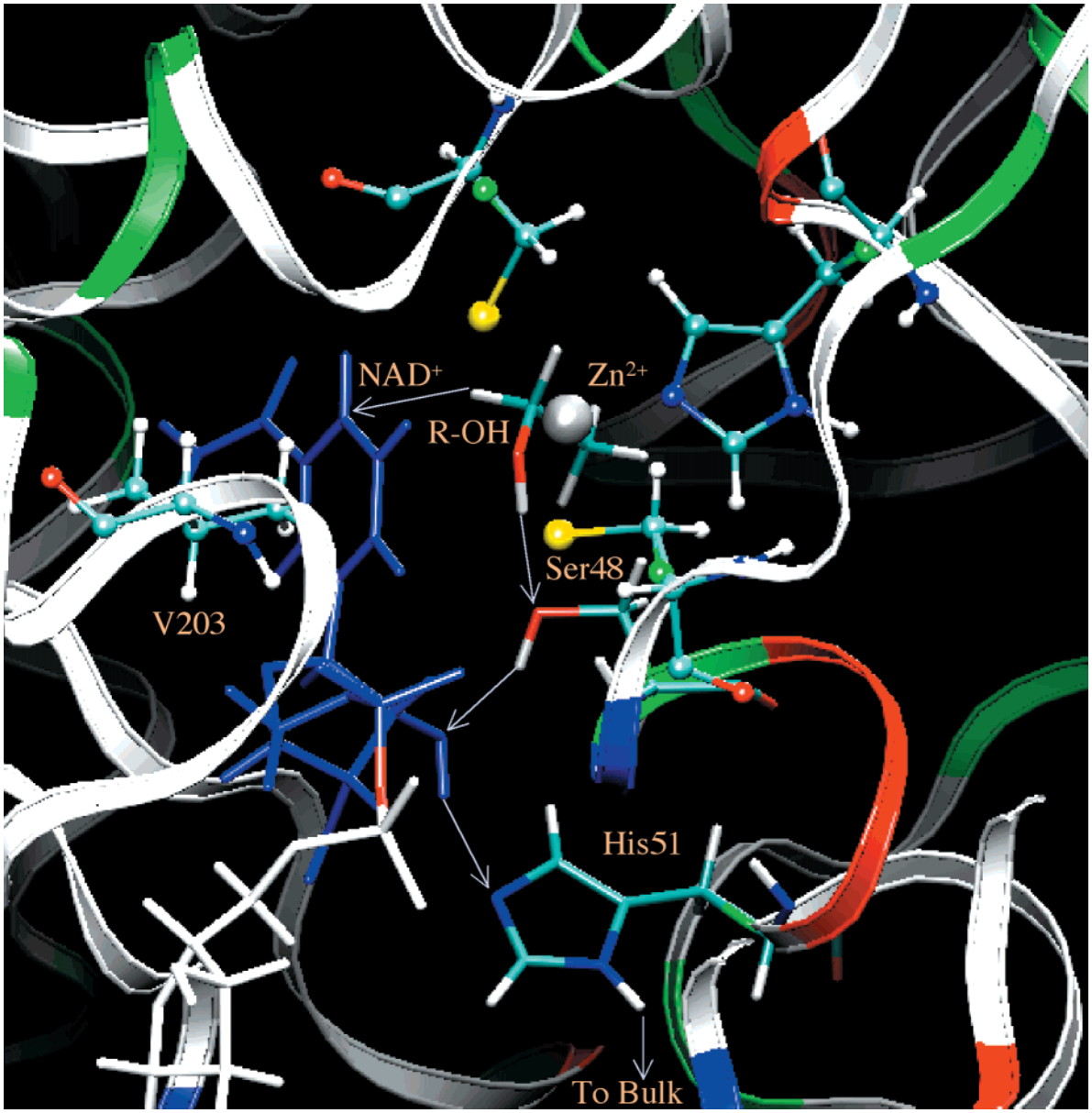

Figure 1. Active site of horse liver alcohol dehydrogenase with important residues. The protein residues (Ser 48 and His 51) and the substrate (ethanol), which are involved in the proton and hydride transfers and therefore treated with QM (SCC−DFTB), are shown as stick models; the blue part of the cofactor NAD^+ was also treated with QM. The catalytic zinc ion and its ligands (Cys 46, Cys 174, and His 67), which are shown in the ball-and-stick representation, were treated with QM. The residue V 203, which is in close contact with the nicotinamide ring in NAD^+, is also shown in ball-and-stick; it was treated with MM. The rest of the protein environment, which was treated with the CHARMM 22 force filed, is shown in a ribbon form, which is color-coded according to the residue types: nonpolar (white); polar (green); basic (blue), and acidic (red). The figure was made with the program VMD (Humphrey, W.; Dalke, A.; Schulten, K. *J. Mol. Graph.* **1996**, *14*, 33).

by Klinman and co-workers[15] with the inhibitor trifluroethanol replaced by ethanol was used for the simulation.

The proton/hydride transfer steps (see Scheme 1) were initially followed by adiabatic mapping using $s = (r_{D-H} - r_{A-H})$ as the approximate reaction coordinate, where D and A are the hydride/proton donor and acceptor, respectively. These adiabatic mapping calculations were done in a *stepwise* manner, such that only one proton or hydride was moved while the other hydrogen bonds involved in the translocation chain were fixed at their equilibrium distances. Two sets of mapping sequences were tested; one follows the sequence **PT1**, **PT2**, **PT3**, and **HT** and the other follows **PT3**, **PT2**, **PT1**, and **HT** (see Scheme 1). The structures obtained from the adiabatic mapping calculations were then used in the optimization of the transition states with the conjugate peak refinement method[45] in CHARMM. Minimum energy paths were determined from the calculated saddle points by following the steepest descent path with the TRAVEL module of CHARMM to confirm their connection with the proper stable states. For selected structures (including **R**, **INT1**, **INT2**, **TSH**, and **P** in Figure 2), single-point energy calculations at the level of B3LYP[46]/CHARMM with a DZP quality basis set (6-31G** for the main group elements[47] and 12s6p4d basis for zinc[48]) were carried out at HF/3-21G/CHARMM optimized geometries. The optimization at the HF/CHARMM level was terminated when the RMS gradient was smaller than 0.1 kcal/(mol Å), which required about 100 minimization steps starting from SCC−DFTB/CHARMM optimized structures. For **TSH**, the value of the antisymmetric stretch coordinate, *s*, was set to −0.2 Å during the geometry optimization. The major differences between B3LYP//HF−CHARMM and SCC/CHARMM results are that the proton transfer steps are more exothermic (by 10.3 kcal/mol for PT1 and merely 2.1 kcal/mol for the subsequent

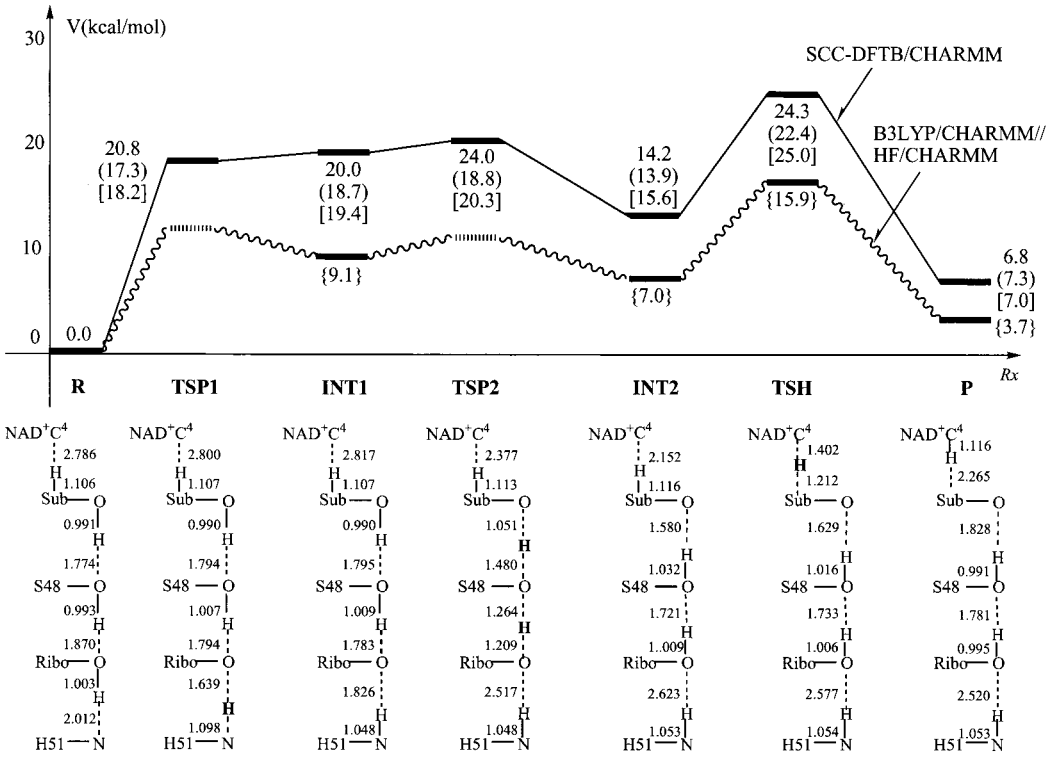

Figure 2. Schematic potential energy profiles for the proton/hydride transfer paths computer at the SCC−DFTB/CHARMM level, and important geometrical parameters of the critical stationary points. The SCC−DFTB region consists of 79 atoms that are involved in the proton/hydride transfer (see text). Electrostatic corrections based on Poisson−Boltzmann calculations were included (see text and ref 19). The values are the minimum and transition states; the values in the parentheses include zero-point corrections and the values in the brackets are effective free energies obtained by adding vibrational free energy contributions (including 278 atoms around the active site). The absolute energy for the reference structure **R**, used as the zero of energy, is −114.48114 hartree; the zero-point correction is 2.17634 hartree, and the vibrational free energy is 2.06660 hartree. The numbers in curly brackets are single-point energy obtained with B3LYP/DZP/CHARMM at HF/3-21G/CHARMM optimized structures, including the electrostatic corrections and vibrational contributions evaluated at the SCC−DFTB/CHARMM level. The absolute B3LYP/DZP/CHARMM energy for **R** is −4270.91548 hartree. The stability of structures **INT1** relative to the reactant is underestimated at the SCC−DFTB/CHARMM approach because SCC−DFTB overestimates the deprotonation energy of ethanol compared to imidazole (See Supporting Information). The associated proton-transfer transition state, **TSP1**, therefore, is expected to be stabilized at the B3LYP/DZP/CHARMM as well, relative to the SCC−DFTB/CHARMM results. The relative stabilities of **INT2** and **INT1** are very similar at the two levels. Thus, the concerted feature of the associated proton transfers found at the SCC−DFTB/CHARMM level is expected to be correct (see text).

PTs) and the hydride transfer step is less exothermic (by 5.3 kcal/mol) at the former level; the trend is consistent with that observed in the gas-phase model calculations (see Supporting Information). To analyze the effects of individual amino acid residues on the reaction energetics in LADH, a perturbation analysis[49] for selected steps were carried out at the SCC−DFTB/CHARMM level.

Kinetic modeling was carried out for the entire set of proton, hydride transfer reactions in LADH to determine if there is significant accumulation of intermediates. This is important for identifying the rate-limiting steps and for an unequivocal comparison of the results with experimental measurements of the kinetics (e.g., whether the observed rate constant is for hydride transfer or coupled proton/hydride transfer; see discussions in section III.1). Similar to the previous analysis of TIM,[49] both exact analytic solutions[50] and steady-state approximations were used for the coupled unimolecular reactions in the enzyme. The rate constant for each elementary step was obtained from transition-state theory (TST), including the vibrational free energies calculated for each stable species and transition state; the effect of tunneling was neglected because it was found to be small at room temperature (see section III.2). The dissociation of the product was included in the coupled rate equations (assumed irreversible) with the rate constant taken from ref 8.

Several issues related to the kinetic isotope effects in LADH were analyzed. First, the effect of tunneling was calculated for the hydride transfer step. Based on the potential energy surfaces obtained from current work (see below), tunneling is likely to be less significant for the proton transfers in this system because either the forward (e.g., **INT1** → **TSP2**) or reverse (**INT1** → **TSP1**) barriers are very low since if the barrier is low in either direction, the barrier is expected to be wide, with a low imaginary barrier frequency. For the hydride transfer step, which follows the proton release, His 51 was taken to be singly protonated at the Nϵ position; i.e., the Nδ proton gets released into the bulk after the proton-transfer steps and was deleted from the calculation and the orientation of the water molecule that is hydrogen bonded to His 51 was optimized to account for the change of protonation state of His 51. In the tunneling calculations, Ser 48 and His 51 were treated as composed of MM atoms to reduce the computational cost. The primary and secondary KIEs (and mixed isotope effects, see Table 1 footnote) were computed at several levels including transition-state theory (TST), canonical variational transition-state theory (CVT), and the canonical variational transition-state theory with small curvature semiclassical tunneling (CVT−SCT).[21,51,52] As described in detail previously,[51,53] a part of the classical dynamical correction to TST (i.e., recrossing of the transition state) is included in variational TST by allowing the position of the transition state deviate from the saddle point; in CVT, the transition state is defined as the maximum on the free energy profile along the minimum energy path. In CVT−SCT, the

TABLE 1: Kinetic Isotope Effects for the Hydride Transfer Step with the SCC−DFTB/CHARMM Potential[a]

kinetic isotope effects[b]		TST[d]	CVT[d,g]	SCT−CVT[d]	exptl[d]
primary	k_H^H/k_T^H	(3.81) 3.13 [2.71]	(3.56) 3.03 [2.72]	(5.91) 4.54 [3.70]	(10.8) 7.15/7.76[e]
	k_D^H/k_T^H	(1.51) 1.42 [1.37]	(1.47) 1.42 [1.39]	(1.81) 1.73 [1.66]	
	k_D^D/k_T^D	(1.55) 1.43 [1.39]	(1.50) 1.43 [1.38]	(1.69) 1.57 [1.50]	(2.02) 1.89/1.86[e]
	α_P^H	(3.41) 3.37 [3.33]	(3.28) 3.18 [3.01]	(2.98) 2.75 [2.57]	
	α_P^D	(3.08) 3.08 [3.06]	(3.13) 3.11 [3.10]	(3.40) 3.34 [3.23]	(3.4) 3.1/3.3[e]
secondary	k_H^H/k_H^T	(1.08) 1.08 [1.08]	(1.10) 1.09 [1.08]	(1.39) 1.27 [1.19]	(1.39) 1.33/1.33[e]
	k_H^D/k_H^T	(1.02) 1.02 [1.02]	(1.02) 1.02 [1.02]	(1.08) 1.06 [1.05]	
	k_D^D/k_D^T	(1.02) 1.02 [1.02]	(1.02) 1.02 [1.02]	(1.06) 1.05 [1.04]	(1.05) 1.07/1.05[e]
	α_S^H	(3.19) 3.12 [3.04]	(4.62) 4.02 [3.46]	(4.20) 4.15 [3.57]	
	α_S^D	(3.50) 3.39 [3.20]	(4.81) 4.50 [4.07]	(5.30) 5.20 [4.67]	(7) 4.1/6.1[e]
solvent[c]	$k_{Ser48-OH}/k_{Ser48-OD}$	0.87			0.50[f]

[a] Atoms within 6 Å from the C_α atom in the substrate, i.e., 278 atoms, were allowed to move in the rate constant calculations. All bound vibrational degrees of freedom were treated with quantum mechanical vibrational partition functions. See section II for a description of the method used. [b] Rate constants are represented in the format: $k_{primary}^{secondary}$ where "secondary" and "primary" refer to the hydrogen position. The primary and secondary Swain−Schaad exponents are defined as the following: $\alpha_P^I = \ln(k_H^H/k_T^H)/\ln(k_D^I/k_T^I)$ and $\alpha_S^I = \ln(k_H^H/k_H^T)/\ln(k_I^D/k_I^T)$, where I = H or D. [c] In the solvent KIE calculations, the hydroxyl hydrogen of Ser48 was taken as a proton or a deuterium. [d] Values without parentheses or brackets are for 300 K; those with parentheses and brackets are for 250 and 350 K, respectively. [e] Values without parentheses are for benzyl alcohol oxidation at 300 K, from ref 15; due to the presence of kinetic complexity, the values are believed to be lower limits. The value before the slash is for the wild-type enzyme, and that after the slash is for the mutant F93W in which hydride transfer is believed to be rate-limiting. The numbers with parentheses are for benzyl alcohol oxidation at 253 K for the mutant F93W in 40% MeOH from ref 68. Note that there is substantial uncertainty (about 3) in the secondary Swain−Schaad exponent at 253 K. The effect of MeOH (which was not included in the simulation) is not clear. [f] From ref 17 for ethanol oxidation. [g] The optimized positions for the transition state (in mass-weighted atomic unit) along the reaction path in CVT for different isotope combinations at (250), 300, and [350] K are the following. H^1H^2: (−0.079) −0.065 [-0.049]. D^1H^2: (−0.041) −0.032 [-0.023]. T^1H^2: (−0.015) 0.060 [0.086]. H^1D^2: (−0.091) −0.084 [-0.077]. H^1T^2: (−0.090) −0.084 [-0.078]. D^1D^2: (−0.051) −0.042 [-0.034]. D^1T^2: (−0.054) −0.045 [-0.038]. T^1D^2: (−0.012) 0.013 [0.031]. The trend is that a heavier primary isotope makes the transition state later, while a heavier secondary isotope makes the transition state earlier.

effect of tunneling is calculated with a WKB expression through the ground-state vibrational adiabatic potential along the minimum energy path; multidimensional effects (such as "corner-cutting") are included by modifying the reduced mass of the tunneling particle based on the reaction path curvature.[51] The calculational method used here is very similar to that described in ref 21; it differs from that in ref 21 in that all reaction path related properties such as normal modes (computed by finite difference of the analytical first derivatives) and reaction path curvatures are computed with a modified version of CHARMM.[53] As a result, we are able to include 278 movable atoms in the rate constant calculations. This corresponds to all the atoms within a 6 Å sphere around the substrate; for comparison, only 21 movable atoms were included in ref 21. A corresponding study of tunneling in triosephosphate isomerase has indicated that more than one hundred atoms need to be included to obtain reliable results.[53] Since the primary goal here is to investigate the qualitative effect of tunneling on the hydride transfer step, no averaging over different enzyme structures was performed. This is based on the observation from our studies of TIM[53] that tunneling coefficients do not vary significantly if the structure of the environment is not strongly perturbed during the reaction. This requirement is satisfied by the first proton transfer in TIM, for example, and by the hydride transfer in LADH. A very small variation (e.g., 0.9 out of 6.2 for the H/T kinetic isotope effect) in the kinetic isotope effects was observed in ref 21 for different active site geometries.

The temperature dependence of the kinetic isotope effects was also examined. The calculation makes use of a reaction path determined by energy minimization, so that the effective potential surface is independent of temperature; i.e., the variation as a function of temperature in the kinetic parameters arises from the motion on that surface due to changes in the vibrational contributions. For a more complete estimate of the temperature dependence, the reaction path itself would have to be determined at different temperatures; calculations with more extensive configurational sampling are left for future. It should be noted, however, that the donor−acceptor distance is allowed to relax during the reaction and is an important part of the reaction coordinate in the current calculations. Therefore, the potential used here is not the same as that referred to in some analyses,[26] in which a "rigid" system is used where no donor−acceptor distance change or vibrational excitation is included.

To examine the solvent KIE, the hydroxyl proton of Ser 48 was replaced by deuterium. Although tunneling is expected to be important for the *substrate* isotope effect, we do not expect tunneling to be significant for the *solvent* isotope effect and therefore restricted calculations to the level of TST in that case. In other words, we do not expect that the tunneling coefficient for the hydride transfer will be affected by the isotope substitution on Ser 48. In TST and tunneling calculations, the bound vibrational motions (e. g., those involving the motion of the hydroxyl proton in Ser 48) are treated with quantum mechanical partition functions.

To consider the effect of structural flexibility on the overall catalysis, rather than on the tunneling for which it is expected to be small (see above), *classical* potentials-of-mean-force (PMF) were computed for the hydride transfer step at a number of temperatures. This was done to see if the change in the flexibility of the protein has any significant effect on the energetics of the hydride transfer. We note that this corresponds to an equilibrium effect rather than a dynamic effect (see section III.3). The QM region used in the tunneling calculation (see above) was employed. The PMF was obtained with umbrella sampling technique[54] using $s = (r_{D-H} - r_{A-H})$ as the reaction coordinate. Twenty windows were sampled at each temperature, and the centers of the windows ranged from −1.2 to 1.2 Å. In each window, 20 ps of molecular dynamics was carried out and the first 5 ps was treated as equilibration and excluded from the analysis. The dynamics was calculated with combined MD/LD (Langevian dynamics) consistent with the stochastic boundary method.[41] The weighted histogram method[55] was used to obtain the potential of mean force over the entire range. The PMF calculations were carried out at 200 K and 300 K to

determine the temperature dependence of the reaction and compare them with the available measurements; the temperature 200 K was chosen here because a dynamical transition exists for many proteins at 220 K and has been investigated by simulations.[56,57] Thus, even though there exist no measurements at this temperature, it was of interest to determine whether the low-temperature resulted in any characteristic behavior. To estimate the uncertainty in the results, calculations starting from different initial conditions (either different initial velocity distributions or different initial coordinates) were carried out. Further, the PMF was computed with a number of *mixed* temperature simulations to probe the role of thermal fluctuations, particularly those in the environment, on catalysis. In these calculations, the QM region and the MM region were associated with different thermostats using the Nose−Hoover algorithm[58] in CHARMM. Three such simulations with 300 K/200 K, 200 K/300 K and 300 K/100 K were carried out; the value before the slash is the temperature for the QM region.

It should be emphasized that because only the chemical steps are studied in the current work, we discuss the catalytic behavior of LADH in terms of k_{cat}. This, or better, the ratio of k_{cat} to k_{uncat}, the uncatalyzed rate in solution gives a direct measure of how the chemical steps of the reaction are accelerated by the enzyme. It has been pointed out by a referee that the "catalytic efficiency" of an enzyme is typically expressed in terms of k_{cat}/K_M.[1] This is a different quantity, which is not of primary interest for the present analysis. However, it should be noted that a quantitative comparison between the calculated k_{cat} and the measured value is not straightforward because the chemical steps are only partially rate-limiting; i.e., there appears to be significant kinetic "complexity" in the reaction.[4,14,15]

III. Results and Discussion

III.1. Mechanism for the Proton and Hydride Transfers. *SCC−DFTB Results.* Figure 2 shows the schematic potential energy surface and important geometrical parameters along the proton/hydride transfer pathways (see Scheme 1); active site structures are shown in the Supporting Information. For the three proton transfers, only two saddle points were found and the results were shown to be insensitive to the initial adiabatic mapping sequence; i.e., when the sequence PT3, PT2, and PT1 was followed in the adiabatic mapping and the results optimized with CPR, the lower energy pathway (PT1, PT2, and PT3) was obtained. In **TSP1**, the 2′-ribose proton is already transferred to the Nδ of His 51 with a H···Nδ distance of 1.098 Å and a H···2′-O distance of 1.639 Å. The other two protons hardly moved during the PT1 step; i.e., their O−H distances are very similar to those in the reactant (see Figure 2). For the subsequent proton transfers, a nearly *concerted* saddle point, **TSP2**, was located. The hydroxyl proton in Ser 48 is halfway between the 2′-O of NAD^+ (1.209 Å) and the Oγ of Ser 48 (1.264 Å). The proton in the substrate has moved significantly toward the acceptor oxygen (Oγ in Ser 48): the H···Oγ distance is 1.480 Å relative to the value of 1.795 Å in **INT1**, and the alcohol O···H distance is 1.051 Å relative to the equilibrium value of 0.990 Å. In the intermediate formed after the proton transfers, **INT2**, Ser 48 is strongly hydrogen bonded to the zinc-bound alcohol; the distance between the OH oxygen in Ser 48 and the alcohol oxygen is only 2.580 Å. The small value is comparable to the result of 2.50 Å from high resolution (1.25 Å) X-ray study on the enzyme complexed with NAD^+ and 2,3,4,5,6-pentafluorobenzyl alcohol (cited as Plapp et al., unpublished in ref 9). The partially concerted behavior found here (also see below) for the proton transfer steps in LADH is fundamentally different from the *stepwise* proton transfers obtained in ref 20a. The difference is likely to be due primarily to the fact that the semiempirical PM3 method used in ref 20a typically overestimates the barrier for proton-transfer reactions.[59]

The transition state for the hydride transfer (**TSH**) is early in that the hydride- donor and acceptor distances are 1.212 and 1.402 Å, respectively. Although the hydride transfer occurs after the proton transfers have taken place, there is still some coupling. The hydrogen bond between Ser 48 and the substrate oxygen is slightly weakened at **TSH**, as manifested by the increase in distance from 1.580 to 1.629 Å (see Figure 2 or 3): a similar result was obtained in the study of an active-site model.[20a] This leads to a calculated H/D solvent isotope which is significantly smaller than unity and therefore supports the argument that the hydride transfer is coupled to the proton motion along the translocation chain[9] (see section III.3). As observed in previous work,[20a] the planarity of the NAD ring varies as the hybridization state of the C^4 atom changes in the hydride transfer reaction (see Figure 3). The $C^4-C^3-C^2-C^6$ dihedral angle (see Scheme 1 for atomic labels) is 3.9° in **INT2**, 9.5° in **TSH** and 12.5° in the product; the corresponding $C^4-C^5-C^6-C^2$ angle is 4.9°, −10.1°, and −12.3°, respectively. The $N^1-C^2-C^3-C^5$ dihedral angle also changes substantially during the hydride transfer: it varies from 1.8° in **INT2**, to −5.2° in **TSH** and −8.8° in the final product. The position of the secondary hydrogen is also changed substantially in **TSH** relative to **INT2**: e.g., the $H_2-C_\alpha-C_\beta$ angle is 110.5 and 113.3° in **INT2** and **TSH**, respectively, and the $H_2-C_\alpha-C_\beta-O$ is 122.9 and 135.3°, respectively (see Figure 3). Therefore, there is "coupled motion" between the secondary and primary hydrogen along the reaction path (see section III.2). To examine the possibility that the H transfer to NAD^+ is a radical mechanism, the splitting between the singlet and triplet states at the saddle point was calculated at the B3LYP/6-31+G(d,p) level (because the current implementation of SCC−DFTB does not allow unrestricted high-spin calculations); the value is more than 60 kcal/mol, which rules out the possibility of a radical mechanism.

Zero-point energy (ZPE) and the vibrational contributions to the free energy at 300 K have a substantial influence on the qualitative reaction profile (see Figure 2). Barriers are lower when ZPE is included and the effect ranges from 1.6 kcal/mol for the hydride transfer (measured from **INT2** to **TSH**) to 3.9 kcal/mol for the concerted PT2, PT3 (measured from **INT1** to **TSP2**). Compared to the saddle points, the relative energetics of the stable structures are less affected by the inclusion of ZPE. As a result, although there are two saddle points on the potential energy surface for proton transfer, only one (**TSP2)** remains when ZPE was taken into account; i.e., the energy of **INT1** (18.7 kcal/mol relative to the reactant) is higher than **TSP1** (17.3 kcal/mol) with ZPE included. The vibrational contribution to the effective free energy is relatively small, on the order of 1 kcal/mol for the various steps (see Figure 2). This is consistent with the fact that the reactions considered involve only localized structural changes of the protein. On the effective free energy surface (Figure 2), the proton-transfer barrier (**TSP2**) was calculated to be 20.3 kcal/mol relative to the starting structure; the intermediate after the proton transfers, **INT2,** was 15.6 kcal/mol. The barrier for the hydride transfer was 9.4 kcal/mol from **INT2**, and the final product was 7.0 kcal/mol above the starting structure. The hydride transfer barrier from the reaction path calculations is very similar to the value of 9.8 kcal/mol from PMF calculations (see below), once again reflecting the local nature of the hydride transfer.

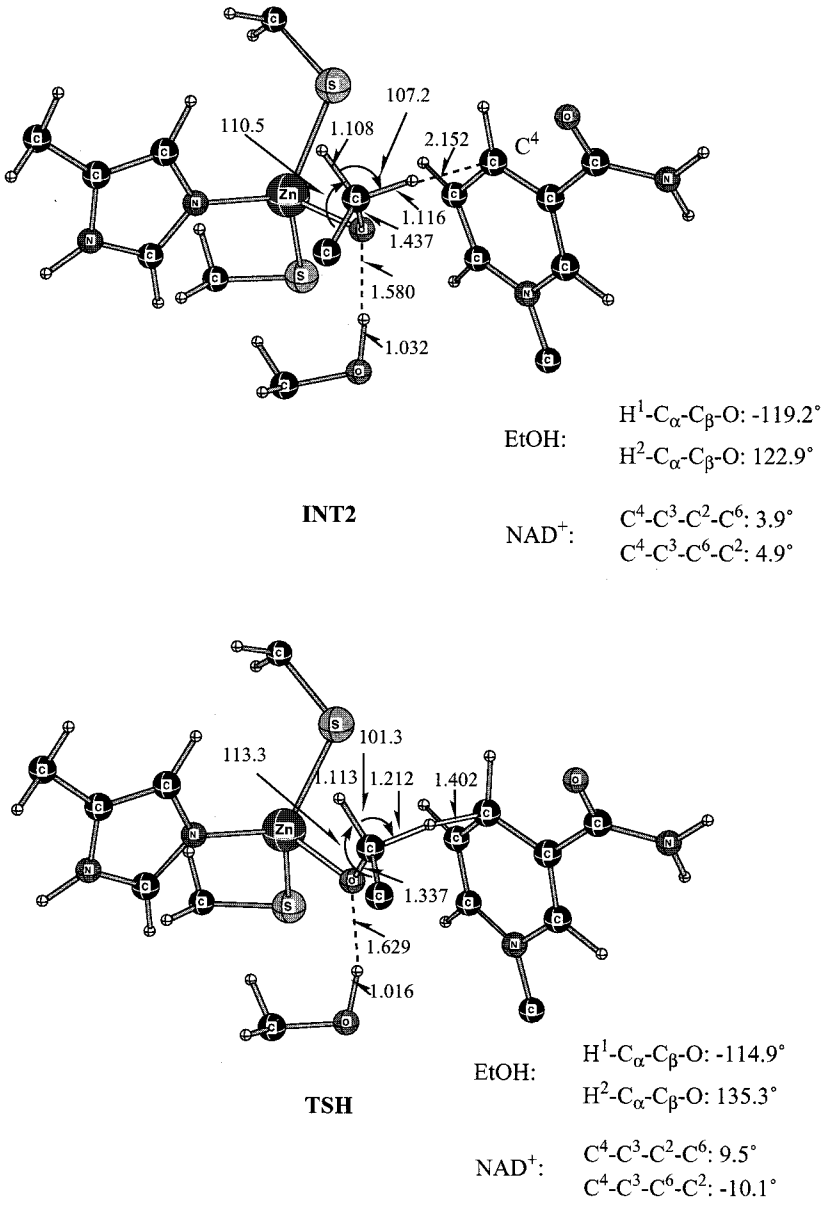

Figure 3. Active site structures for the reactant (**INT2**) and saddle point (**TSH**) for the hydride transfer reaction obtained at the SCC−DFTB/CHARMM level. Some atoms (e.g., the H atoms on the Cβ in the substrate) were omitted for clarity. The change in the geometrical parameters related to the secondary hydrogen in the substrate and the deviation from planarity of the NAD^+ ring are of interest (see text). Distances are in angstroms, and angles are in degrees.

DFT Results. Although previous calculations suggest that SCC−DFTB typically gives superior results compared to commonly used semiempirical methods such as AM1 and PM3, it may have substantial error for some reactions (e.g., the protonation affinity of imidazole; see Supporting Information).[32] Therefore, it is crucial to test the accuracy of the method in the study of each system. For this purpose, single-point calculations were performed at the B3LYP/CHARMM level with HF/3-21+G/CHARMM optimized structures (see Method). The results are given in Figure 2 along with those at the SCC−DFTB/CHARMM level. At the B3LYP/DZP/CHARMM level, the two intermediates are substantially stabilized relative to the reactant, by as much as 10.3 kcal/mol for **INT1** and 8.6 kcal/mol for **INT2**. In other words, the error in the SCC−DFTB/CHARMM results is mainly associated with the first proton-transfer step, and the subsequent steps are well described; e.g., the stability of **INT2** relative to **INT1** is only overestimated by 1.7 kcal/mol. This is consistent with the observation that SCC−DFTB overestimates the deprotonation energy of ethanol relative to imidazole (see Supporting Information). Since the SCC−DFTB/CHARMM calculations substantially underestimate the stability of **INT1**, it is expected (according to Hammond's postulate) that the barrier associated with the first proton transfer step is overestimated: i.e., the first proton transfer might have a nonvanishing reverse barrier and therefore be separated from the subsequent proton transfers at a higher level of theory, such as B3LYP/CHARMM. However, the concerted behavior found for PT2 and PT3 at the SCC−DFTB/CHARMM level is expected to be qualitatively correct, because the energetics between **INT1** and **INT2** are well-described at this level. Thus, the calculations (at the SCC−DFTB/CHARMM and B3LYP/CHARMM levels) indicate that the proton transfers in LADH are concerted with the atoms arranged close to the X-ray configuration, although there is some ambiguity for the first proton transfer.

Although we found that the transfer of the second and third proton to be concerted, the behavior could be modulated by the conformation of the fluctuating protein. The proton transfers

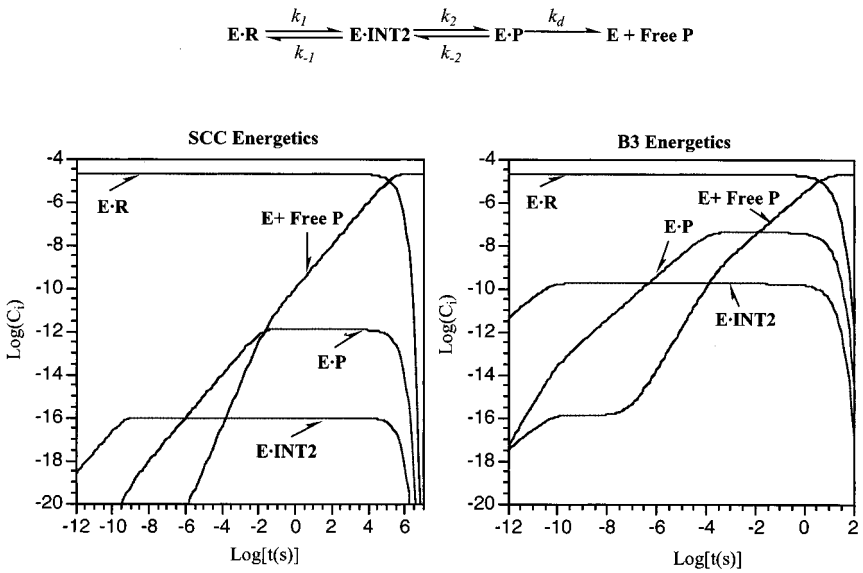

Figure 4. Concentrations of a number of species (E·**R**, E·**INT2**, E·**P**, and E + free **P**) as a function of time obtained from the analytical solution of the coupled unimolecular proton-transfer reactions. The initial concentration of [E·**R**] was set to 20μM. The rate constants associated with the chemical steps were derived from TST using the effective free energies from SCC−DFTB/CHARMM or B3LYP/CHARMM calculations (Figure 2); the contribution of tunneling was not included due to the small absolute effect (see text). The preexponential factor was set equal to k_BT/h; this may not be exact, but it is only a scale factor; the rate constants calculated at the B3LYP/CHARMM level are: $k_1 = 2.2 \times 10^5$ s^{-1}; $k_{-1} = 2.6 \times 10^{10}$ s^{-1}; $k_2 = 2.3 \times 10^6$ s^{-1}; and $k_{-2} = 9.3 \times 10^3$ s^{-1}. The dissociation rate constant for **P** was taken from ref 8, which is 79 s^{-1}. Note that because structural change in the enzyme upon NAD$^+$ binding was not modeled in the current work, it is not appropriate to compare the kinetic behavior with experimental measurement (e.g., ref 14).

are expected to be less concerted if larger distances between the donor and acceptor oxygen atoms make a significant contribution to the equilibrium population. In a model study, it was found that proton transfer along a water-chain can be either stepwise or concerted depending on the relative water configurations generated by molecular dynamics simulation with restraints.[60] Also, for carbonic anhydrase, the behavior of the proton transfers (concerted or stepwise) was found to be sensitive to the number of bridging water molecules (Cui and Karplus, unpublished).

The hydride transfer step has a barrier of 8.9 kcal/mol at the B3LYP/DZP/CHARMM level, similar to the SCC−DFTB/CHARMM result of 9.4 kcal/mol. The hydride transfer step is less exothermic by about 3.3 kcal/mol at the B3LYP/DZP/CHARMM level as compared to SCC−DFTB/CHARMM calculations, which is also consistent with the difference between SCC−DFTB and B3LYP results on gas phase models (see Supporting Information). In the previous studies, the calculated barriers for the hydride transfer are substantially higher. In ref 20a, the barrier was obtained from a B3LYP/6-31G** calculation on HF/3-21G optimized structures with an active site model consisting of 148 atoms. Due to the absence of the enzyme environment, rather large, probably artificial, geometrical changes occurred during the hydride transfer (see Table 3 in ref 20a); e.g., the Ser 48 fragment seems to have moved substantially away from the substrate during the reaction. Furthermore, the hydride-acceptor distance is 3.62 Å in that model, which is much larger than the value of 2.15 Å found in our study. Since it is well-known that the barrier for proton and hydride transfer reactions depends sensitively on the donor−acceptor distance, it is not clear if the obtained value in ref 20a can be quantitatively related to the barrier in the enzyme. In another study,[21] a more complete model for the enzyme (similar to the current work but without the charge scaling procedure) was employed, but a less sophisticated QM treatment was used and the parameters were adjusted such that the barrier for the hydride transfer step corresponded to the kinetic measurements. As described below, our calculations suggest that it may not be appropriate to relate the hydride transfer barrier directly to the kinetic measurements, because the hydride transfer appear not be decoupled kinetically from the proton transfer (see below).

Kinetic Modeling. As shown in the kinetic modeling results in Figure 4, the concentration of **INT2** reaches a steady state in about 1 ns with either SCC−DFTB/CHARMM or B3/CHARMM energetics, and the steady-state concentration remains small (10^{-16} M with SCC−DFTB/CHARMM and 10^{-10} M with B3LYP/CHARMM); the initial concentration for the Michaelis complex used in the kinetic modeling was 20 μM, although the time-dependence of the reaction (absolute values do depend) does not depend on the initial concentration because only unimolecular steps were considered.[8,9] We note that because structural changes in the enzyme upon NAD$^+$ binding was not modeled in the current work, it is not appropriate to compare the kinetic behavior (Figure 4) with experimental measurement (e.g., ref 14). The small steady-state concentration for **INT2** is due to its high energy (15.6 and 7.0 kcal/mol at the SCC−DFTB/CHARMM and B3LYP/CHARMM levels, respectively). At the SCC−DFTB/CHARMM level, the apparent barrier height is 25.0 kcal/mol, which is significantly larger than that observed experimentally (∼16.9 kcal/mol) with ethanol as the substrate.[8,61] At the B3LYP/DZP/CHARMM level, by contrast, the apparent barrier height and endothermicity of the overall reaction are 15.9 and 3.7 kcal/mol, respectively; these are in good agreement with the experimental estimate of 16.9 and 1.6 kcal/mol, respectively.[8] At both levels, the exact solutions agree well with the steady-state results, and the apparent barrier height is related to the free energy difference between **TSH** and the reactant. Therefore, although the current reaction path calculations are only expected to be semiquantitative, the results seem to suggest that the hydride transfer and proton transfers are *not* separated kinetically, i.e., **INT2** appears not to accumulate substantially (see below for the pH dependence of the reaction). There is no direct experimental evidence indicating that the proton transfers are kinetically decoupled

from the hydride transfer. As a result, it is not clear if it is appropriate to adjust the potential parameters such that the hydride transfer barrier fits the measured kinetics, as done in ref 21. However, the effect of such adjustment on the calculated tunneling appears to be small (D. G. Truhlar, private communication).

pH Dependence. The pH dependence of the LADH catalyzed oxidation has been studied experimentally. It was found that the rate of benzyl alcohol oxidation is most rapid above a pH value of 6.4 or 8.4.[10,62] In addition, the position of the internal equilibrium between benzyl alcohol and benzyl aldehyde was found to exhibit a complex pH dependence with pK_a values of 6.5 and 8.1.[8] For ethanol as the substrate, the enzyme exhibits a bell-shaped pH dependence for k_{cat}/K_M, and an almost pH-independent k_{cat}.[63] The pH dependence for ethanol can be fitted with two ionizable groups with pK_a's of 6.7 and 9.0: two likely candidates are the zinc-bound alcohol and His 51, although their precise pK_a values were difficult to determine experimentally (it has not been determined from experiments which is which, although a recent measurement[9] for a doubly mutant in which His 51 is no longer involved in the proton relay suggests that the value around 6.4 is likely for the zinc-bound alcohol). Kvassman and Pettersson studied the pH dependence of trifluoroethanol, and obtained a pK_a value of 4.3. They found that trifluoroethanol dissociates faster from the protonated form of the enzyme, and therefore attribute the observed pK_a value to the zinc-bound alcohol.[10]

The pK_a value for the zinc-bound alcohol, which by definition is related to the free energy for the proton transfer from the alcohol to the bulk solution, was estimated using the free energy difference between **INT2** and the reactant (ΔG(**R**→**INT2**)); i.e.,

$$pK_{EtOH\cdot Zn} = \Delta G(\mathbf{R}\rightarrow\mathbf{INT2})/2.303k_BT \qquad (1)$$

The approximation made in eq 1 is that the subsequent proton transfer from **INT2** to the bulk solvent, which was not modeled in the current study, does not make substantial contribution (i.e., nearly thermoneutral); this assumption seems consistent with the calculated pK_a of His 51 in INT2 (vide infra). The above procedure was followed instead of the standard Poisson−Boltzmann technique[64] because extensive rearrangements in the hydrogen bonds take place after the deprotonation of the alcohol. Such determined pK_a value for the substrate ethanol is 5.7 at the B3LYP/DZP/CHARMM level. To determine the pK_a value for His 51, the standard Poisson−Boltzmann method[64] and Monte Carlo sampling technique[65] was employed. The pK_a value was 5.5 in the starting structure, **R**, and 8.1 in **INT2**; i.e., at neutral pH, His 51 is likely to be singly protonated in **R** and doubly protonated in **INT2**. This behavior is consistent with Scheme 1; i.e., His 51 prefers to be singly protonated in **R** at pH = 7 such that Nϵ can serve as the acceptor in the hydrogen bonding interaction with the OH group in the ribose of NAD^+; in **INT2**, by contrast, His 51 prefers to be doubly protonated (at pH = 7) such that NϵH can serve as the donor group in the hydrogen bonding interaction with OH in the ribose. The interaction matrix from the PB results indicates that several nearby ionizable groups, including Arg 47, Asp 49, Asp 50, Glu 267, Arg 363, and Arg 369, also interact strongly with His 51 and therefore influence the pK_a of the latter. At pH lower than 5.5, according to the current results, the substrate alcohol (estimated pK_a of 5.7, see above) and His 51 are likely to be singly and doubly protonated, respectively, in the reactant state. Thus, it is expected that the activity of LADH is low at pH lower than 5.5: this is in qualitative agreement with experimental observations[10,62] for ethanol and also for benzyl alcohol. At pH higher than 8.1, His 51 will be in the single protonation state in both **R** and **INT2**. Calculations with the singly protonated His 51 (also used in the hydride tunneling calculations, see Method) suggest that the hydride transfer barrier (measured relative to **INT2**) is hardly affected by the protonation state of His 51. This is consistent with the observation that k_{cat} for the ethanol substrate is almost pH independent between 6.7 and 9.0.[63] However, a direct comparison is not possible because k_{cat} is dominated by NADH release in the experimental measurement. At very high pH, the favorable free energy corresponds to the deprotonation of His 51 (His^+ to His) can stabilize **INT2** substantially such that the intermediate is lower in free energy compared to the reactant and therefore accumulates during the reaction. In this case, the hydride transfer is kinetically decoupled from the proton transfers; the current results at the B3LYP//HF/CHARMM level at neutral pH (Figure 2) indicates that this is unlikely to occur under physiological conditions.

Perturbation Analysis. As shown in Figure 5, a number of charged groups make large contributions to the energetics of proton and hydride transfers in LADH. The important groups include Arg 369, Asp 49, Glu 68, and NAD^+, as well as the structural zinc ion and its ligands (Cys 100, 103, and 111). The NAD^+ strongly disfavors the first proton transfer, and also slightly disfavors the hydride transfer; it substantially favors the second and third proton-transfer steps, by about 7 kcal/mol with respect to the stability of **INT2** relative to **INT1**. The positively charged Arg 369 favors the proton transfer reactions, but disfavors the hydride transfer step. Its effect is compensated by the two negatively charged residues, Asp 49 and Glu 68, which disfavor the proton transfers but favor the hydride transfer reaction. They make significant contributions to several steps of the reaction as shown in Figure 5. In addition to the charged residues, several polar groups such as Thr 56 and the main chain of Ser 48, Val 292, Val 294 as well as several X-ray resolved water molecules close to His 51 (e.g., Solv 81 and 157 and Solv 16) also play important roles, especially for the first proton transfer which involves the protonation of His 51. There are no experimental data concerning the importance of Asp 49, Glu 68, and Arg 369 for the chemical steps in LADH. It clearly would be of interest to have mutation studies for these residues. It is interesting to note that for yeast alcohol dehydrogenase, in which the chemical step is believed to be rate-limiting[4,18] (e.g., the isotope effects on k_{cat} and k_{cat}/K_M are similar for wild type and several mutants), the mutant E68Q was found experimentally to have a k_{cat} value that is nearly 40 times smaller than that of the wild type (9.9 and 360 s^{-1}, respectively).[66] The interpretation of mutation result for LADH is more complicated due to the fact that the reaction is partially limited byproduct release (i.e., by "kinetic complexity"), and therefore it is difficult to probe directly the role of a residue in the proton/hydride transfer. For example, it was found that mutant I269S has a higher activity than the wild type for certain alcohols, and it was argued that this is due to the fact that the mutation affects the dissociation of the product,[67] which is partly rate-limiting.

III.2. Kinetics Isotope Effects in LADH. *Effect of Tunneling on the Hydride Kinetic Isotope Effects.* One of the primary reason for the focus on LADH is that it has become a model system for experimental studies of tunneling effects in enzymes, as discussed in the Introduction. In the experimental analysis, it is assumed that the measurements reflect hydride tunneling, even though there is some "complexity",[14,15] which refers to the fact that the chemical step is not fully rate-limiting. The effect of hydride tunneling on the absolute value of rate constant

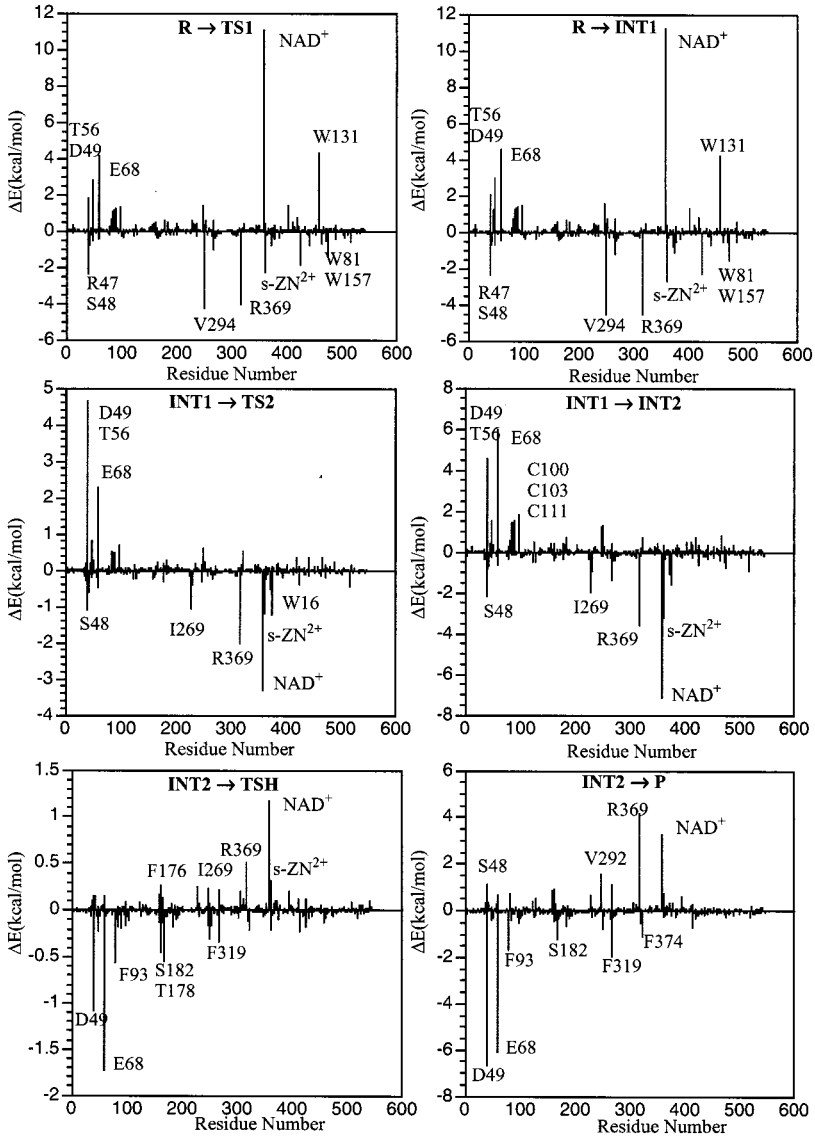

Figure 5. Perturbation analysis for the proton and hydride transfer reactions in LADH at the SCC−DFTB/CHARMM level. The contribution to a particular reaction for each residue is defined as the energy difference caused by zeroing out the partial charges of this residue. A *negative* value indicates that the residue contributes favorably to a given step. The differences in energy scales of the figures should be noted. All energies are in kcal/mol.

at 300 K is calculated to be rather small (2.08 when both the primary and secondary positions are H). However, tunneling is found to have a significant effect on the KIEs and the Swain−Schaad exponents (SSE). The results at 300 K are similar but not identical to those of Alhambra et al.[21] Table 1 shows the calculated values at three temperatures (see Method) for the primary isotope effects and the corresponding SSEs. The calculated values of the isotope effects and the SSEs are reasonably close to the experimental measurements for benzyl alcohol,[15,68] at both 300 and 250 K; no values are available for ethanol. Also, it should be noted that the measurements of 250 K were done in 30% methanol; the effect of this is not known. In all cases, there is a monotonic decrease in the primary kinetic isotope effect with increasing temperature, as expected; for the secondary isotope, there is also a monotonic behavior, except that for TST and CVT, the results are essentially unaffected by temperature between 250 and 350 K.

For the primary position, as also observed and discussed in the study of TIM,[53] the SSE is not necessarily raised when tunneling is included. This was noted by Rucker and Klinman, who stated, "Positive deviations from this range (3.26−3.34) are considered to be an indication of tunneling, although the expected magnitudes of such deviations have been difficult to quantify".[26] In fact, the SCT−CVT gives smaller exponents compared to the TST or CVT values; the latter are close to the classical[69] limit of 3.3. Nevertheless, the SCT−CVT gives larger temperature dependence of the primary SSE, which is consistent with the fact that tunneling does play an important role. In agreement with ref 21, the representative tunneling energy (defined as the energy at which the product of the transmission coefficient and the Boltzmann factor is a maximum) indicates that the hydride transfer occurs by tunneling under the vibrationally adiabatic barrier by only 0.3 kcal/mol at 300 K. Therefore, the dominant tunneling path is not expected to deviate substantially from the minimum energy path at room temperature. As the temperature decreases, however, tunneling paths that cut the corner of the minimum energy path are likely to be more significant.[20b,51] A more quantitative evaluation of this aspect of the reaction will be presented elsewhere (Cui and Karplus, unpublished).

One difference from ref 21 is thathydride tunneling is "normal" in the current calculations in the sense that $\kappa_H > \kappa_D$

$> \kappa_T$. An abnormal trend, $\kappa_T > \kappa_D > \kappa_H$, was found in ref 21: it was mentioned that this has been observed before[70] and was thought to be due to the multidimensional character of the tunneling event. It is not clear whether the difference in the two sets of calculations is due to the different potential functions or to different numbers of movable atoms included in the rate constant calculations.

For the secondary position, it is seen that even TST and CVT give H/T KIEs significantly different (1.08−1.09) from unity, suggesting that the secondary hydrogen is involved in determining the transition-state structure and barrier frequencies. As mentioned in section III.2, the secondary hydrogen has changed its position considerably in the saddle point compared to the reactant (see Figure 3); i.e., there is clearly "coupled motion" involving the secondary and primary hydrogen along the reaction path.Therefore, the secondary substitutions may affect the position of the transition state (see the footnote of Table 1). The general trend is that secondary substitution with a heavier isotope leads to an earlier transition state (optimized in CVT; see Method). For example, the donor−hydride distances are 1.200 and 1.187 Å for the substrate with H and T on the secondary position, respectively; the acceptor-hydride distances are 1.420 and 1.452 Å, respectively. The planarity of the NAD^+ ring is also slightly affected; e.g., the $C^4-C^5-C^6-C^2$ dihedral angles decreases from −7.4 to −6.6° when the secondary position is substituted with T (see also discussions in section III.1). We note that the values quoted here are slightly different from those in Figure 3 even when the secondary position is hydrogen, because the transition state (optimized in CVT as the maximum on the free energy profile along the reaction path) deviates slightly from the saddle point (values for the latter are shown in Figure 3); see the footnote of Table 1.

The calculated secondary kinetic isotope effects indicate that tunneling at the primary position is affected substantially by the secondary substitution. For example, the secondary H/T effect at 300 K is 1.09 and 1.27 at the CVT and SCT−CVT level, respectively. This is in agreement with the result of ref 21. As shown there, this effect is due mainly to the fact that the adiabatic barrier critical for tunneling is wider and the reaction path is less curved when the secondary hydrogen is substituted by tritium. For example, in the present calculations, the barrier frequency decreases from 783i to 734i cm^{-1} upon tritium substitution at the secondary position; these values are somewhat lower than those in ref 21, which are 1046i and 1002i cm^{-1}, respectively. Moreover, the secondary H/T effect obtained with a tunneling model without the effect of the reaction path curvature is much smaller (1.15 compared to 1.27 at 300 K). The secondary SSEs obtained here are different from those in ref 21. First, as the position of transition state is optimized (i.e., with CVT), the secondary SSE increases from the TST value of 3.1 to about 4.0 at 300 K, which is much closer to the experimental values; it should be noted, however, that it has been suggested that the actual secondary SSE is larger, in that the experimental value reflects kinetic complexity. In the calculations of ref 21, the CVT value (3.4 ± 0.4) for the secondary SSE is also larger than the TST value (3.3 ± 0.2), although the difference is smaller.

The effect of mixing primary and secondary isotopes[26,71] (i.e., using protonium at the *primary* position in measuring secondary H/T kinetic effect, but deuterium when considering the secondary D/T kinetic effect) is rather small at the TST and CVT levels for both the primary and secondary kinetic isotope effects (Table 1); i.e., the rule of the geometric mean (RGM)[72] is a good approximation in LADH without tunneling. With tunneling included at the SCT−CVT level, the RGM broke down,[71] and the effect is larger for the primary kinetic isotope effect. For example, k_D^H/k_T^H and k_D^D/k_T^D are 1.73 and 1.57 at 300 K, respectively. These results are in accord with the fact that the magnitude of tunneling becomes smaller (1.85 vs 2.08 at 300 K) when the secondary hydrogen is substituted with a heavier isotope, as discussed above. The effect of mixing primary and secondary isotopes is much smaller on the secondary kinetic isotope effect. Due to the smaller value of the D/T secondary kinetic isotope effect, however, mixing isotopes has a somewhat larger effect on the secondary SSEs, relative to the primary SSEs. For example, α_P^H and α_P^D at 300 K are 2.75 and 3.34, respectively; α_S^H and α_S^D are 4.15 and 5.20, respectively.

The calculated KIEs and SSEs presented in this section suggest that although hydride tunneling is important for the kinetic isotope effects in horse LADH, the effect of tunneling on the absolute rate constant is small (about 2 at 300 K); the qualitative behavior is very similar although not identical to those found in ref 21. Moreover, although tunneling has a substantial effect on the values of SSEs, other factors such as the variations in the position of transition state upon isotope substitution also have a significant influence. The latter arises from the fact that the motion of the secondary hydrogen is part of the reaction coordinate and therefore secondary substitution changes the character of the transition state, including geometry, energetics, barrier frequency and reaction path curvature. The changes in the geometry and energetics (as reflected in CVT) have a nonnegligible influence on the rate constant and therefore kinetic isotope effects. Thus, as emphasized in the previous study,[53] one has to be very cautious in correlating the values of SSEs to the magnitude of tunneling. This aspect of our conclusion is different from that in ref 21 and 26; the latter two suggest that the deviation of the secondary SSE from the "classical" limit of 3.3 is due entirely to tunneling. In particular, it should be noted that the value 3.3 is not a classical[69] limit for *secondary* SSE because the zero-point energies involving the secondary atoms are largely conserved at the transition state.[53] In the current calculation for LADH, TST happens to give a value close to 3; by contrast, in several proton-transfer reaction in TIM,[53] values close to 4 were obtained at the TST level. In ref 26, a very small classical secondary kinetic effect (1.014 for the secondary H/T effect, which is much smaller than the TST values obtained here or in ref 21) and a large contribution of tunneling (which gives 1.35 for the secondary H/T effect) were found to be necessary to construct a vibrational model that can reproduce the experimental results for yeast ADH.[73] However, this is likely to be due to the two limitations in the treatment;[26] i.e., a simple one-dimensional expression[74] was used for tunneling, which usually overestimates the tunneling contribution, and the position of the transition state was not allowed to change upon secondary isotope substitution.

Kinetics of Mutants. Recently, kinetic measurements on a number of mutants were made in which the binding pocket of NAD^+ was perturbed.[14,15] Although NADH release is rate-limiting in wild-type LADH, the chemical step (*assumed* to be hydride transfer, in agreement with the observed isotope effect and the present calculation) is believed to be mostly rate-limiting in mutants perturbing the V203 position, especially with a second mutation F93W. An approximately linear relationship was observed between the k_{cat}/K_M value and the *secondary* Swain−Schaad exponent, $\ln(k_H/k_T)/\ln(k_D/k_T)$. This was interpreted as reflecting a correlation between the magnitude of tunneling and catalytic efficiency. The interpretation was based on the assumption that the secondary SSE correlates with the

magnitude of tunneling. However, the present results and our previous calculations on triosephosphate isomerase[53] showed that the assumption is not generally valid. Indeed, such an assumption also is not fully consistent with the measured kinetic data. For example, the V203G mutant was said to have the smallest tunneling contribution because it has the smallest secondary Swain−Schaad exponent.[15] However, the *primary* isotope effects (both k_H/k_T and k_D/k_T), which are quantities that correlate well with the magnitude of hydride tunneling (e.g., as found in our previous calculations for TIM[53]), are not smaller for V203G than for other mutants. They are actually larger than both the V203A and L57F mutants, which have substantially larger secondary SSEs and also larger k_{cat}/K_M values. Thus, the interpretation of the mutant data appears to be more complex than was assumed in the original analysis. Moreover, it is not clear to us why one should correlate k_{cat}/K_M with the hydride transfer kinetic isotope effect rather than with k_{cat} itself since there is no rational for expecting a large isotope effect on K_M. Moreover, it is stated in ref 15 "The reduction in the rate for Val-203 mutants in consistent with a *chemical* step that has become rate-limiting...We conclude that the hydride transfer step is likely to be fully rate-determining with Val-203→ Ala".[15] It seems surprising, therefore, that for the mutants considered in ref 15, the variations in K_M (ranges from 0.028 to 2.1 mM) are much larger than those in k_{cat} (from 0.12 to 0.24 s^{-1}) except for the surprisingly large value of 1.8 s^{-1} for the V203A mutant. Of course, the issue of kinetic complexity can make the interpretation of the experiments and their comparison with our calculations more difficult.

Solvent Isotope Effect. As described in section III.1., the hydrogen bond distance between Ser 48 and the substrate oxygen increases from 1.580 to 1.629 Å after the hydride transfer, because the carbonyl oxygen is a weaker hydrogen bond acceptor than carboxyl oxygen. This leads to the calculated H/D solvent isotope effect of 0.87 (Table 1) at the TST level with quantized bound vibrations. Although larger than the experimental value of 0.5,[9,17] it is significantly smaller than unity (which would be found if the vibrational mode involving the substituted isotope were not perturbed during the reaction) and therefore supports the suggestion that the hydride transfer is coupled to the proton motion along the translocation chain.[9] The larger value of the computed solvent KIE is due partly to the fact that SCC−DFTB usually underestimates the strength of the hydrogen bonds;[32,33] i.e., SCC−DFTB underestimates the hydrogen-bonding interaction between Ser 48 and the substrate oxygen in **INT2** and the degree by which this interaction is weakened due to the hydride transfer.

III.3. Effect of Structural Fluctuations on Catalysis. There can be both equilibrium and dynamic (nonequilibrium) contributions from the *fluctuating* protein environment to the reaction rate, in correspondence with the solvation effects on reactions in solution at finite temperatures.[75] If the chemical step is significantly slower than the rate at which the instantaneous barrier height is modulated by different enzyme configurations, the rate of the chemical process can be obtained from the potential of mean force (PMF) along the reaction path.[76,77] The PMF, which is an equilibrium property, is largely determined by the mean geometrical arrangement of the reacting groups (such as the mean proton donor−acceptor distance) and the mean electrostatic field in the enzyme active site, which in turn are affected by the surrounding protein and environment. The averaged protein structure can be affected by external conditions such as temperature and also possibly by structural changes (such as decrease in flexibility) induced by mutation or other modification (such as glycosylation[5a]). However, it should be noted that the PMF is not that the potential energy profile corresponds to the mean structure since it is determined by averaging the energies over the structures with Boltzmann weights. In the other limit, where the time scale for the enzyme to sample different configurations (leading to different instantaneous barriers for the chemical step) is longer than the chemical step, the introduction of a PMF is no longer appropriate and it is necessary to average the "instantaneous" rate constants over the Boltzmann-weighted enzyme configurations; the appropriate weighting would be obtained from a molecular dynamics simulation.[31] Such a scenario was found appropriate, for example, for CO rebinding in myoglobin at low temperature or in a highly viscous solvent.[76,78] This regime also has been shown to occur in enzymes at room temperature by single molecule techniques,[79] although the changes in the structure of the enzyme, which occur on a millisecond time scale, have not yet been characterized. It is possible that relaxation of the enzyme after the reaction has taken place also plays a role in the observed behavior.[80]

The contribution of dynamics, which can be characterized by the transmission coefficient, deals with the effect of protein motions (or the instantaneous protein configuration when the barrier crossing time scale for the chemical step is short, relative to the protein relaxation time, as in proton-transfer reactions[31]) on the dynamical behavior of the reacting groups, e.g., recrossing of the transition state. The nonequilibrium effect is modulated by the relative time-scale of the protein motion and barrier crossing events of the reacting groups, the coupling between the chemical process and protein motion ("friction" in the GLE framework) and its dependence on the reaction coordinate.[81] The magnitude of such (classical) dynamic effects has been found to be rather small in magnitude. It was found to reduce the rate by about a factor of 2, for example, in the first proton-transfer step in triosephosphate isomerase[31] and probably is rarely greater than a factor of 10, except in nonadiabatic reactions. Quantum dynamical effects, such as tunneling, can play an important role in H transfer reactions. These generally increase the rate of the reaction, though again a factor of 10 appears to be near the upper limit at room temperature. This has been described in section III.2. It has also been suggested that enzyme can favor specific type of motions of the substrate, therefore making an entropic contribution, whose effect on the rate constant would be approximately temperature independent of the catalytic power and the stereospecificity;[82,83] this possibility is not examined here.

Effect of Structural Flexibility on the Hydride Transfer. Here, we focus on the possible role of protein motion (flexibility) on the *equilibrium* aspects of enzyme catalysis. Classical potentials-of-mean-force (PMF) for the hydride transfer step were computed at 200 and 300 K with different initial conditions (either different initial velocity distributions or different initial coordinates). Further, the PMF was computed using *mixed* temperature simulations in which the QM region and the MM region were associated with different thermostats (300 or 200 K) using the Nosé−Hoover algorithm[58] in CHARMM. The main purpose is to reveal any possible connection between the flexibility of the protein, the averaged active-site structure and the energetics (barrier) of the chemical step (hydride transfer) catalyzed by the enzyme; a corresponding simulation analysis has been employed to examine the protein and solvent contribution to protein dynamics.[56] The calculations in section III.2 indicates that although hydride tunneling is important for the quantitative interpretation of the kinetic isotope effects, the absolute effect

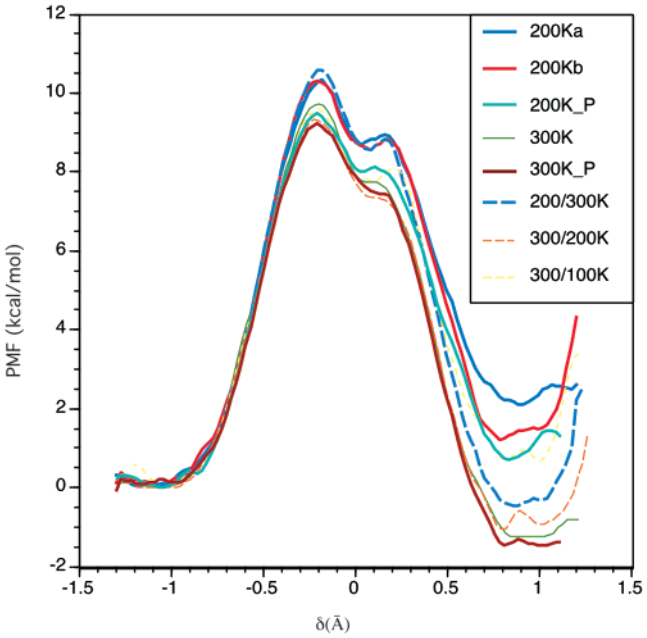

Figure 6. Potential of mean force (PMF), in kcal/mol, for the hydride transfer step in wild-type LADH from simulations at different temperatures as a function of the reaction coordinate δ (defined as the antisymmetric stretch involving the donor, C_α in EtOH, acceptor, C^4 in the NAD^+ ring, and the hydride atoms; this applies to all the δ in other figures) in angstroms. The solid lines are from uniform temperature simulations, and the dotted lines are from mixed temperature simulations in which the QM region and MM region are associated with different thermostat (see Method). The "_P" set of calculations started from the product ($NADH + EtO^-$), while the others started from the reactant ($NAD^+ + EtOH$).

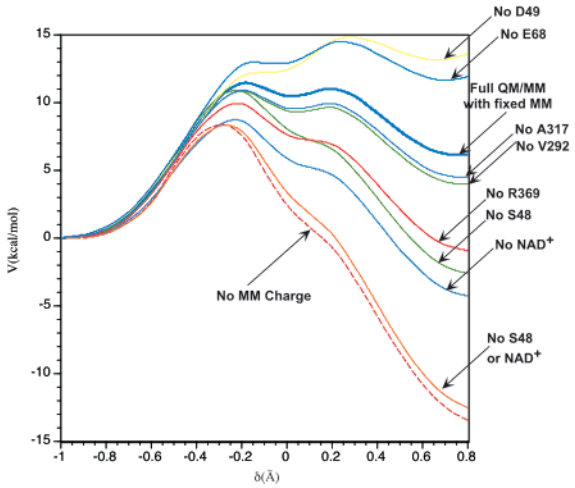

Figure 7. The effects on the energetics of the hydride transfer as a function of the antisymmetric stretch as the approximate reaction coordinate (see Methods and the caption of Figure 6) from zeroing the partial charges of several MM residues. The MM environment was fixed at the average product state from the mixed temperature 200/300 K simulation.

of tunneling on catalysis is not significant at room temperature for LADH (a factor of 2). This observation suggests that useful information can be obtained by using classical molecular dynamics to investigate the possible connection between structural fluctuations and catalysis in LADH. More quantitative studies, including a study of the effect of tunneling with path-integral molecular dynamics, are in progress.

Figure 6 shows the potential of mean force along the antisymmetric stretch coordinate relevant to the hydride transfer. The PMF barrier is lower when the temperature of the QM region is higher, although the effect is 1 kcal/mol or less. For example, all simulations with the QM region at 200 K have barriers of 10.5−10.8 kcal/mol, while simulations with the QM region at 300 K have barriers in the range 9.5−9.8 kcal/mol. When the calculations were carried out in the reverse direction (i.e., from the final product state to the reactant state of the hydride transfer), the PMF barriers are lower by 0.5 kcal/mol; the barrier at 300 K is also lower than that at 200 K. The MM temperature has a relatively smaller influence on the barrier height, which is consistent with the argument that the barrier for proton and hydride transfer reactions is mainly determined by the average donor−acceptor geometry; i.e., there is little correlation between the fluctuations of the MM atoms and the motion of the donor and acceptor atoms. For instance, the minimum of the PMF occurs at $\delta = -1.05$ Å and -1.18 Å at 300 and 200 K, respectively; i.e., the average donor−acceptor distances are about 2.16 and 2.29 Å, respectively, assuming a similar average C−H distance of 1.11 Å at the two temperatures and an average linear arrangement of the donor, hydride and the acceptor atoms. The temperature of the MM region appears to be more important for the exothermicity of the reaction, which has a somewhat larger variation in the different simulations. For example, the reaction is *endothermic* in the two uniform 200 K simulations, but is slightly *exothermic* when the QM region is set to 200 K with the MM temperature set to 300 K. Similarly, when the QM region is set to 300 K, the reaction is substantially more endothermic for the MM region at 100 K than at 200 or 300 K. Further, one notes that there is a small bump (~0.5 kcal/mol) in the PMF, which is more visible in cases where the QM region has a low temperature (see below). Several charged and polar residues (e.g., Ser, 48, Asp 49, Glu 68, and Arg 369 as well as NAD^+) were found to be responsible for this small bump; excluding Ser 48 or NAD^+ in the QM/MM calculations make the bump disappear nearly completely (Figure 7). To understand the origin of the bump observed for PMF (Figure 6), the Mulliken charges along the reaction path were examined for the key atoms in the hydride transfer, and the results are shown in Figure 8. It is interesting to note that the transferring "hydride" actually is *positively* charged within the Mulliken scheme; nevertheless, the value ($<+0.13$) is considerably less positive than a transferring proton (e.g., the substrate proton in **TSP2**), which has a Mulliken charge of +0.36. Interestingly, we see a lag in the charge variation on the acceptor carbon (C^4 in NAD^+) and the transferring H atom; i.e., the former reaches a peak at $\delta \sim -0.2$ Å (around the saddle point) and the latter reaches the maximum positive value much later (at $\delta \sim 0.0$). This might explain why negative residues (such as Asp 49 and Glu 68) stabilize the region after the hydride transfer transition state, while positive residues (such as NAD^+, Arg 369, and Ser 48) have destabilizing effects; the latter contribute mainly to the bump on the PMF and the adiabatic mapping potential (see below).

To further investigate the relationship between the energetics and the structural and other equilibrium properties of LADH, as hinted at by the PMF results, more analyses were done for a selected set of PMF trajectories. Since the energetic effects are more evident for the product than those of the transition state, the analyses were carried out only for the reactant and product states (defined by the 20 ps window from PMF simulations with $\delta = -1.05$ and $\delta = +0.9$ Å, respectively). The key question is what residues have substantially different positions in these simulations, and among those, which are responsible for the difference in energetics.

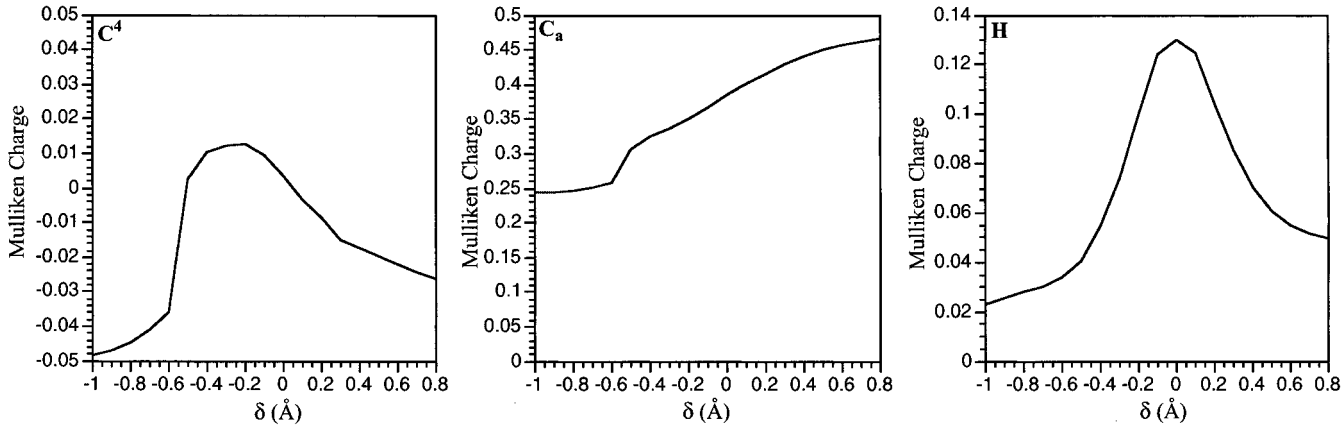

Figure 8. The Mulliken charge on the acceptor (C^4 in NAD^+), donor (C_α in the substrate ethanol) and the transferring hydride along the hydride transfer path.

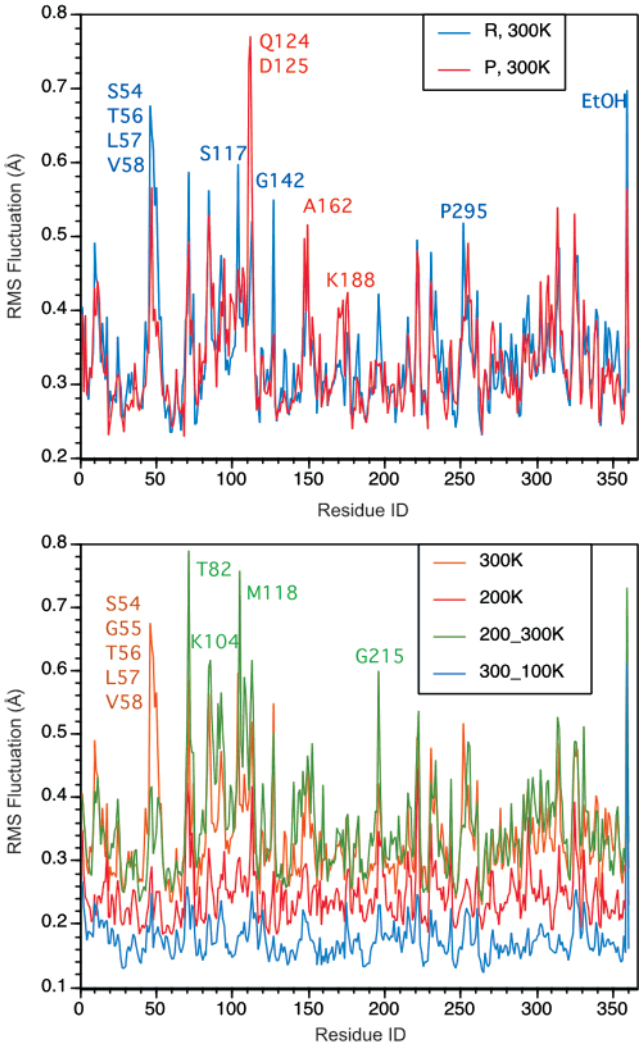

Figure 9. RMS fluctuations of the C_α atoms in LADH and the hydride transfer donor (ethanol C_α atom) and acceptor (C^4 in the cofactor NAD^+) from MD simulations (20 ps window in the PMF calculations). (a) Reactant and product states at 300 K. (b) Reactant state as a function of various temperature regimes.

First, we focus on the structural properties. The RMS fluctuations of selected simulations are shown in Figure 9. A few particularly mobile regions are observed, which include Ser 54−Val 58, Ser 117−Asp 125 and Pro 296−Gln 299: these are all on the surface of the enzyme in the current setup. The substrate was also found to be rather mobile, which is consistent with the small size of ethanol. These trends in the motional behavior are generally similar in the reactant and product states (Figure 9a), and also consistent among different sets of simulations at different temperatures (Figure 9b); some residues (e.g., Gln 124 and Asp 145) have significantly larger fluctuations in the product state. It is interesting to note that the mixed temperature simulation with the QM region at 200 K and MM at 300 K gave somewhat smaller fluctuations for the Ser 54−Val 58 region compared to the uniform 300 K simulation. Comparing the averaged structures for different states (reactant or product) from different simulations, it was found that the major differences occur in these flexible regions. For example, the averaged reactant and product state from the uniform 300 K simulation differ substantially in the region Pro 296−Ser 298 and Leu 116−Gln 124 (Figure 10a); the position of the substrate and NAD^+ are also rather different (>1 Å displacement). A similar situation was found for the product state from the uniform 300 K simulation and the reactant state from the 200/300 K calculation (Figure 10b). For comparison, reaction path minimization only gave substantial displacement of the substrate and NAD^+ (Figure 10c). The fact that reaction path minimization and PMF calculations gave rather similar energetics suggest that the displacement in the flexible region is either not important for the catalysis or the effect averages out in the simulation.

To determine whether the observed structural differences have an effect on the energetics for the hydride transfer step, several adiabatic mapping calculations were carried out using the antisymmetric stretch (see Method) as the approximate reaction coordinate starting with the averaged reactant- or product-state structures obtained from different simulations. The environment (MM part) was either allowed to relax (Figure 11a) or fixed (Figure 11b). The general trend is rather similar but more apparent in the fixed-environment calculations, and therefore only these results will be discussed. The MM environment favors the QM product over the QM reactant in the product-state set of calculations, and therefore the reaction is exothermic and the barrier is lower. The barrier for the hydride transfer varies from 7.0 to 9.4 kcal/mol and the *exothermicity* varies from −1.0 to −5.8 kcal/mol. When the environment is fixed to that in the reactant state, the barrier varies from 10.9 to 11.4 kcal/mol and the *endothermicity* is between 3.6 and 6.1 kcal/mol. For simulations with the MM part at 300 K, the averaged product state has a MM environment that stabilizes the QM product even more and therefore they have substantially larger exothermicities than other simulations with a lower MM temperature.

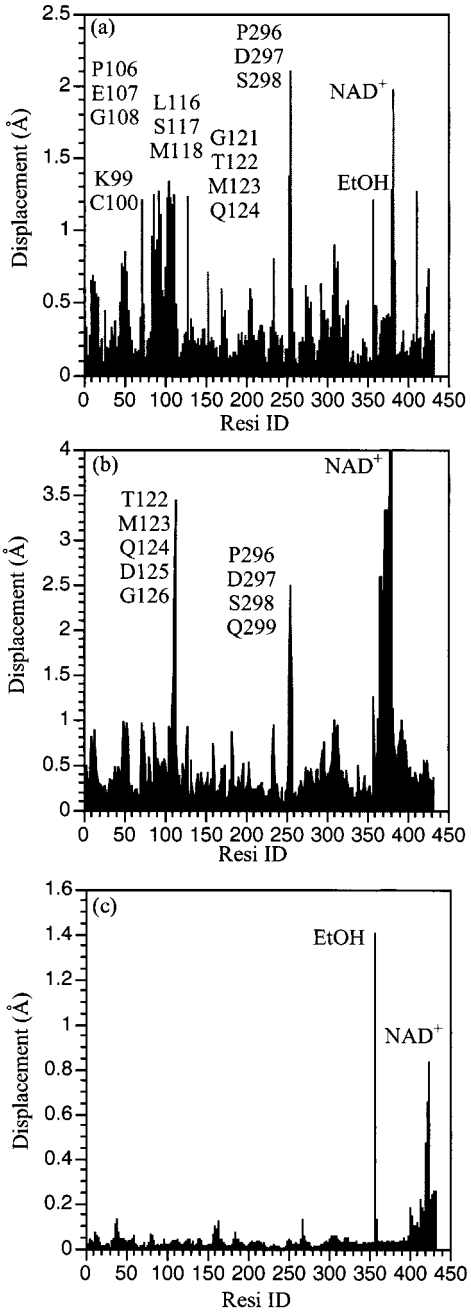

Figure 10. Difference in the atomic positions for structures obtained from various simulations. (a) Difference between the reactant and product-states from the 300 K simulation. (b) Difference between the reactant state and the 200/300 K mixed temperature simulation and the product state from the 300 K simulation. (c) Difference between the reactant and product states from reaction path minimizations.

To find which residues make important contributions to the structure-energy relationship just described, the contributions of MM residues to the energy of the hydride transfer reaction were determined using the perturbation analysis.[84] The calculations were carried out for the 300 K product-state structures and 200/300 K reactant-state structures, which gave the largest exothermicity and largest endothermicity, respectively, in the fixed-environment adiabatic mapping calculations. Although a large number of residues have rather different positions in the two structures considered here (e.g., see Figure 10b for a comparison), only a few residues are important for the energetics of the hydride transfer (Figure 12). This is in accord with the "localized" character of the reaction, which only slightly perturbs the enzyme environment. For a given MM environment (either

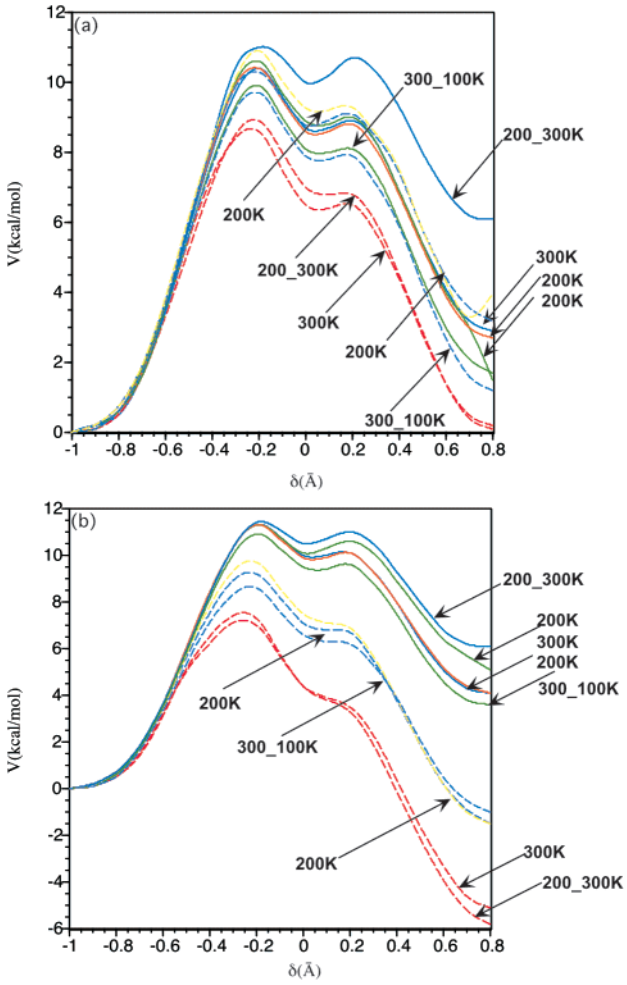

Figure 11. Results from adiabatic mapping calculations for the hydride transfer step using the antisymmetric stretch (see Methods and the caption of Figure 6) as the approximate reaction coordinate starting from structures obtained from different simulations. (a) The MM environment was allowed to relax. (b) The MM environment was fixed at the averaged structure from MD simulations (20 ps window in the PMF calculations). The solid lines started from the reactant-state structures; the dotted lines started from the product-state structures.

300 K product or 200/300 K reactant state), the behavior is very similar to the perturbation result for the structures from the reaction path calculations (Figure 5f). The key residues that substantially favor the hydride transfer (i.e., lower the energy of the product relative to the reactant) are Asp 49 and Glu 68. Several residues such as Ser 48 (which was treated as MM in the PMF calculations) and Arg 369 disfavor the hydride transfer; the phosphate groups of the cofactor NAD^+ are unfavorable. The partial charges on these charged residues (see Methods) were not scaled down due to their proximity to the QM part and their being fully buried, which is one of the reasons that they have large electrostatic and polarization effects. When the results from different sets of simulations are compared (i.e., the differential contribution to the reactions in two sets of simulations at different temperatures, see Figure 12c), the effects from the phosphate groups in NAD^+ cancel out; the cumulative effect from Asp 49, Glu 68, and Arg 369 is also rather small. The most important residue is, therefore, Ser 48, which interacts with the substrate through a short hydrogen bond (see section III.2).

In summary, we have found that the flexibility of the enzyme has an effect on the hydride transfer in LADH. It leads to different averaged MM environments that stabilize the QM region to different degrees. However, the effect is rather local

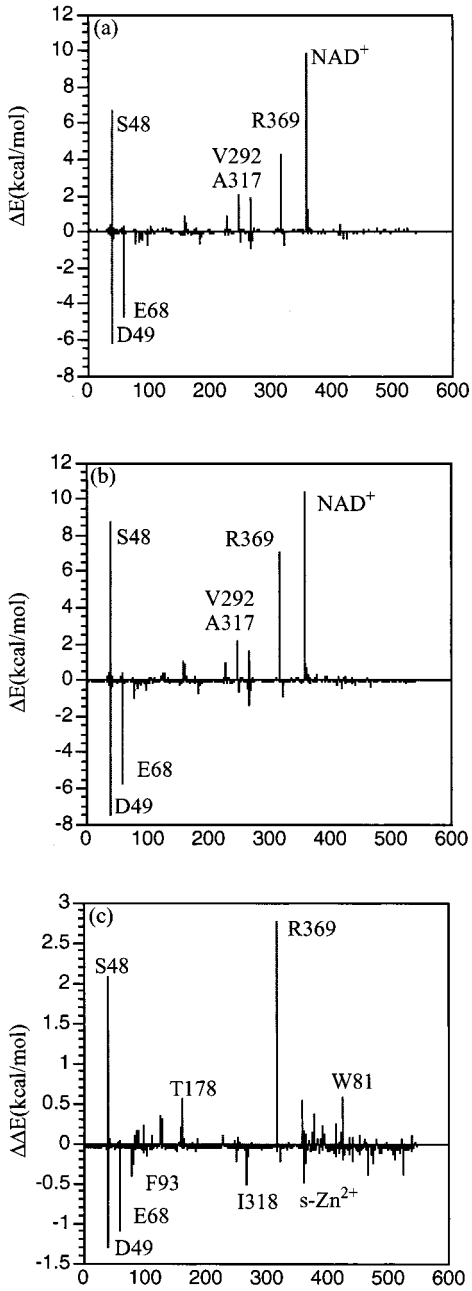

Figure 12. Contributions of MM residues to the energy of the hydride transfer reaction from a perturbational analysis. (a) The MM environment was fixed at the averaged product-state conformation from 300 K simulation. (b) The MM environment was fixed at the averaged reactant-state conformation from 200/300 K mixed temperature simulation. (c) The difference between the contributions of MM residues to the energy of the hydride transfer for the structures in (a) and (b).

and concerns mainly the motion of the QM atoms that are directly involved in the chemical reaction, and nearby groups that interact directly with the QM atoms, e.g., Ser 48 in the current system. The absolute effect appears to be small, on the order of 1 kcal/mol or less. In a recent kinetic analysis of ADH from the thermophillic bacteria *Bacillus stearothermophilus*, Klinman et al.[5b] found that the activation enthalpy increased by nearly 8 kcal/mol when the temperature was lowered from 65 °C to 5−30 °C; the former is the optimal temperature of the thermophile. It was suggested that the flexibility of the enzyme, which is expected to decrease as the temperature deviates from the optimal value,[85] plays an essential role. On the bases of the results for the mesophillic LADH used in the current study, it seems that the classical effect of flexibility is rather small and that the origin of the activation enthalpy change with temperature is more complex[86] than suggested in ref 5c. Because the X-ray structure of the thermophillic ADH is not available, a detailed explanation at an atomic level is still difficult; i.e., there could be a significant structural change. It is possible that the small effect of protein flexibility found here would be increased by the inclusion of zero-point energy and tunneling, which are missing from the current classical potential of mean force calculations and are being investigated. Nonequilibrium effects can also be studied with the activated dynamics approach, and the zero-point and tunneling effects can be approximated by semiclassical (e.g., Wigner) distributions.[87]

Mutation Effect of V203A. Among the several mutants examined,[15] F93W,V203A was found to have one of the smallest k_{cat}/K_M value, which is about 70 times smaller than that of the wild type. The measured values of k_{cat} are very similar, however: they are 0.32 and 0.27s^{-1} for the wild type and the F93W,V203A mutant, respectively. The latter has a substantially larger K_M value of 2.1 mM (that of the wild type is 0.036 mM), which leads to the much smaller k_{cat}/K_M value for the mutant. The smaller catalytic efficiency for the mutant was rationalized based on X-ray data, which shows that the hydride donor−acceptor distance becomes longer as the NAD^+ moves away from the substrate to fill the open space in the binding pocket caused by the mutation. It was also suggested that the interaction between V203 and the NAD^+ has a dynamical effect on the catalysis. For example, the recent classical molecular dynamics simulations by Bruice et al.[82] show that the mutation reduces the production of substrate−NAD^+ conformations that are close to the transition-state structure ("near-attack" conformations). Schwartz et al.[29a] also hypothesized that the V203−NAD^+ vibration is part of the "promoting vibrations" in LADH, although no direct evidence at an atomic level was given. However, all of these effects would be expected to alter k_{cat}, which in fact remains essentially unchanged (but see below), and their role in changing K_M is not clear.

The present reaction path calculations led to a slightly higher hydride transfer barrier of 11.6 (without ZPE) for F93W,V203A, compared to 10.1 kcal/mol for the wild type. Potential of mean force calculations gave a similar trend (see Figure 13). At 300 K, the barrier from PMF calculations is 11.0 kcal/mol for the F93W,V203A mutant, and 9.8 kcal/mol for the wild type LADH. This difference corresponds to a decrease of 8 times in the rate constant for the mutant, according to the TST, at room temperature. It is not straightforward to compare this value directly to the measured k_{cat} because the hydride transfer is not fully rate-limiting in the wild type, but is believed to be rate-limiting in the mutant.[15] Therefore, the measured k_{cat} ratio of 0.32/(0.27∼1.2) is a lower bound for the decrease of the hydride transfer rate due to the mutation. In other words, the current study indicates that the small effect of the mutation on k_{cat} can be accounted for by equilibrium simulations, and that no dynamical effects[29a,82] have to be invoked.

IV. Conclusions

Theoretical calculations have been carried out to study the mechanism of the proton and hydride transfers in horse liver alcohol dehydrogenase. The newly implemented self-consistent-charge density-functional-tight-binding (SCC−DFTB) QM/MM method[32] allowed us to obtain semiquantitative results for not only the adiabatic potential barrier heights, but also for the rate constants, including quantum mechanical effects such as tunneling, and the potential-of-mean-force. The SCC−DFTB/CHARMM appears to be sufficiently accurate for this system

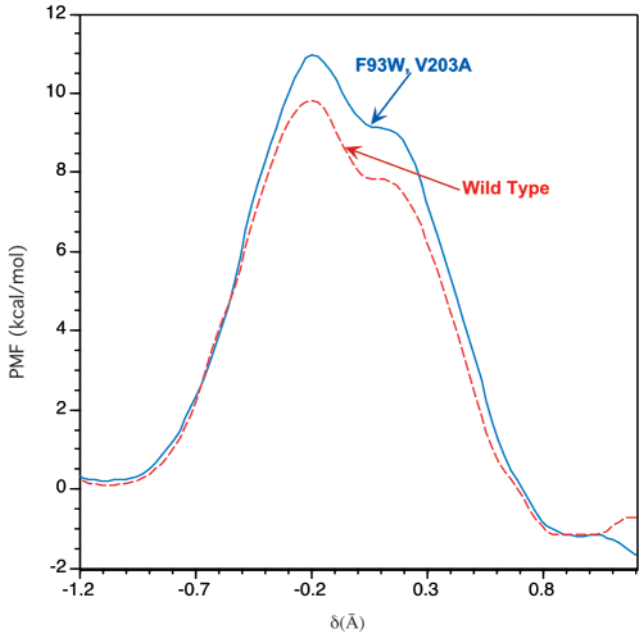

Figure 13. Potential of mean force (PMF) for the hydride transfer step in the wild type and a double mutant F93W, V203A for LADH at 300 K as a function of the antisymmetric stretch (see Methods and the caption of Figure 6) as the approximate reaction coordinate.

to eliminate the need of special parametrization for the system, which had to be used with AM1 for treating triosephosphate isomerase. A reparametrization for the C and H involved in the hydride transfer was made to account for their diffuse electron distribution. The parametrization does not include any LADH related features so that the new parameters should be applicable to hydride transfers in general. They correspond to the need for more diffuse basis sets in ab initio or DFT calculations.[39]

It was shown that the proton transfers proceeds in a virtually concerted fashion before the hydride transfer. This differs from a previous study,[20] which found a stepwise mechanism for the proton transfers; the difference is likely due to the use of the PM3 method, which in general gives too high proton-transfer barrier heights. The intermediate formed after the proton transfer, **INT2**, is not lower in energy than the reactant, which indicates that the proton transfer step and the hydride transfer are not necessarily decoupled kinetically. The situation could be influenced by pH, because **INT2** would be stabilized at high pH by the favorable free energy change corresponding to the proton transfer from the doubly protonated His 51 (the final acceptor along the proton-transfer chain in the protein) to the bulk. The Ser 48 forms a short hydrogen bond with the substrate, which leads to an inversed solvent isotope effect, in qualitative agreement with experiment. The overall apparent barrier and endothermicity from the B3LYP/CHARMM calculations are 15.7 and 3.7 kcal/mol, respectively; these are in qualitative agreement with experiments. The energy splitting between the singlet and triplet electronic states at the saddle point is rather large, which rules out the radical mechanism for the hydride transfer to NAD^+.

The calculated energetics and pK_a values indicate that the chemical steps as reflected by the calculated k_{cat}, are slow for pH lower than 5.5 and the hydride transfer is hardly affected for pH between 5.5 and 8.1; these are consistent with the experimentally measured pH dependence for the reactions catalyzed by LADH although a direct comparison is difficult due to the presence of kinetic complexity in the experiments. A perturbation analysis for the QM/MM energies suggest that a number of charged residues close to the active site (e.g., Asp 49, Glu 68, and Arg 369), as well as the phosphate groups in NAD^+, make important contributions to the energetics of the proton and hydride transfer reactions. It would be of interest to have mutation experiments to test these predictions.

As to the contribution of tunneling and its effect on kinetic parameters, the overall results are similar to those found by Alhambra and co-workers.[21] This is an important result since different potential energy functions were used in the two sets of calculations. Hydride tunneling was found to be very important for the kinetic isotope effects. Including tunneling at the semiclassical ground-state level with the small reaction path curvature approximation gave kinetic isotope effects that are close to experimental measurements. The absolute contribution to the rate constant, however, was found to be small (a factor of 2) at room temperature. A result that is different from the previous studies[21,26] was that the secondary Swain−Schaad exponent can also be affected by the variation in the position of the transition state upon secondary isotope substitution, and therefore does not necessarily reflect the magnitude of tunneling. Although it is possible that accurate secondary Swain−Schaad exponents are more difficult to calculate due to their high sensitivity to the secondary kinetic isotope effects (which tend to be small), the calculated results are consistent. Furthermore, similar trends were observed from different studies.[53] The tunneling contributions for different primary isotopes follow the expected trend of $\kappa_H > \kappa_D > \kappa_T$, while the reverse was found in ref 21. Since both the potential function and the number of movable atoms include in the rate-constant calculations are different from those in ref 21, further study is required to clarify the origin of the difference.

The possible equilibrium effects of protein "dynamics" on the hydride transfer in LADH were studied by potential of mean force calculations under different conditions (uniform and mixed temperatures for the QM and MM region in the enzyme). It was found that flexibility of the enzyme does have some effect on the catalysis because different averaged structures were produced. The effect was rather small in magnitude (<1 kcal/mol), however, and is restricted to the local residues that directly interact with the reacting groups; the most important residue is Ser 48, which interacts with the substrate through a strong hydrogen bond. The results suggest that the large temperature-dependence of the activation enthalpy found in the thermophillic ADH cannot be explained based merely on the change in the flexibility of the enzyme at lower temperatures. Potential-of-mean-force simulations qualitatively reproduced the effect of double mutation, F93W,V203A on k_{cat} of the hydride transfer step, indicating that no dynamical effects have to be invoked[29a,82] for this. However, the origin of the large change in K_M is not clear from the present analysis.

Finally, we emphasize again that only the chemical steps were considered in the present study and that the calculations of these steps were used to evaluate k_{cat} and its dependence on isotopic substitution. Comparisons with experiment were based on the measured values of k_{cat} with the realization that they may not be directly comparable to the calculated values. This is a particular problem in LADH where kinetic complexity is believed to play a role; i.e., the chemical steps are only partially rate-limiting. This problem has clouded the interpretation of experimental isotope effects. Thus, our analysis of the chemical steps, per se, is an essential contribution to trying to understand the kinetics of LADH and related interesting enzymes, which are models for the investigations of tunneling in catalyses. In the future, it would be of interest to also study the binding and

dissociation of the substrate and cofactor (NAD^+/NADH), such that a more direct comparison with experiments can be made.

Acknowledgment. Discussions with Dr. M. Schaefer on the pK_a calculations are gratefully acknowledged. Part of the calculations were carried out on the Origin 2000 SGI machines of Advanced Biomedical Computing Center at the National Cancer Institute. The research was supported in part by the Department of Energy and the National Institute of Health. We appreciate the useful comments made by referees.

Supporting Information Available: The active-site structures for the critical points involved in the proton and hydride transfer reactions in LADH obtained at the SCC−DFTB/CHARMM level are given. The coordinates for these structures can be downloaded from the websites: http://kandinsky.chem.wisc.edu/~qiang/pastprojects/ladh/. Also shown are test calculations (imidazole and ethanol in different protonation states to illustrate the difference between SCC−DFTB and B3LYP methods. Finally, a small active-site model was used to test the accuracy of a specific SCC−DFTB parametrization (for C and H) for hydride transfer reactions, which is required due to the diffuse character of the electron density in those atoms; e.g., a more diffused basis set would be required in the corresponding ab initio or DFT calculations. It should be emphasized that no LADH related models were included in this reparametrization and therefore the new parameters can be used for other hydride transfer reactions. This material is available free of charge via the Internet at http://pubs.acs.org.

References and Notes

(1) (a) Fersht, A. *Structure and Mechanism in Protein Science*; W. H. Freeman and Company: New York, 1999. (b) Radzicka, A.; Wolfenden, R. *Science* **1995**, *267*, 90

(2) Wilson, E. K. *Chem. Eng. News* **2000**, *78*, 42.

(3) Suteliffe, M. J.; Scrutton, N. S. *Trends Biochem. Sci*. **2000**, *25*, 405.

(4) (a) Klinman, J. P. *Crit. Rev. Biochem*. **1981**, *10*, 39. (b) Pettersson, G. *Crit. Rev. Biochem.* **1987**, *21*, 349.

(5) (a) Kohen, A.; Klinman, J. *Acc. Chem. Res*. **2000**, *31*, 397. (b) Kohen, A.; Cannio, R.; Bartolucci, S. Klinman, J. *Nature* **2000**, *399*, 496. (c) Kohen, A.; Klinman, J. *J. Am. Chem. Soc*. **2000**, *122*, 10738.

(6) Eklund, H.; Palpp, B. V.; Samama, J. P.; Brändén, *J. Biol. Chem*. **1982**, *257*, 14359.

(7) Ramaswamy, S.; Eklund, H.; Plapp, B. V. *Biochem*. **1994**, *33*, 5230.

(8) Shearer, G. L.; Kim, K.; Lee, K. M.; Wang, C. K.; Plapp, B. V. *Biochem*. **1993**, *32*, 11186.

(9) Ramaswamy, S.; Park, D. H.; Plapp, B. V. *Biochem*. **1999**, 38, 13951

(10) (a) Kvassman, J.; Pettersson, G. *Eur. J. Biochem*. **1980**, *103*, 557. (b) Kvassman, J.; Pettersson, G. *Eur. J. Biochem*. **1980**, *103*, 565.

(11) Cook, P. F.; Cleland, W. W. *Biochem*. **1981**, *20*, 1805.

(12) Ehrig, T.; Hurley, T. D.; Edenberg, H. J.; Bosron, W. F. *Biochem*. **1991**, *30*, 1062.

(13) Inoue, J.; Tomioka, N.; Itai, A.; Harayama, S. *Biochem*. **1998**, *37*, 3305.

(14) Bahnson, B. J.; Park, D. H.; Kim, K.; Plapp, B. V.; Klinman, J. P. *Biochem*. **1993**, 32, 5503

(15) Bahnson, B. J. Colby, T. D.; Chin, K. J.; Goldstein, B. M.; Klinman, J. P. *Proc. Natl. Acad. Sci. U.S.A.*, **1997**, *94*, 12797.

(16) Schmidt, J.; Chen, J.; DeTraglia, M.; Minkel, D.; McFarland, J. T. *J. Am. Chem. Soc*. **1979**, *101*, 3634.

(17) Sekhar, V. C.; Plapp, B. V. *Biochem*. **1990**, *29*, 4289.

(18) Northrop, D. B.; Cho, Y. K. *Biophys. J*. **2000**, *39*, 2406.

(19) (a) von Onciul, A. R.; Clark, T. *J. Compt. Chem*. **1993**, *14*, 392. (b) Vanhommerig, S. A. M.; Meier, R. J.; Sluyterman, L. A.; Meijer, E. M. *J. Mole. Struct.: THEOCHEM* **1996**, *364*, 33. (c) Cárdenas, R.; Andrés, J.; Krechl, J.; Campillo, M.; Tapia, O. *Int. J. Quantum Chem*. **1996**, *57*, 245. (d) Ryne, U. *Eur. Biophys. J*. **1996**, *24*, 213. (e) Olson, L. P.; Luo, J.; Almarsson, Ö.; Bruice, T. C. *Biochem*. **1996**, *35*, 9782.

(20) (a) Agarwal, P. K.; Webb, S. P.; Hammes-Schiffer, S. *J. Am. Chem. Soc*. **2000**, *122*, 4803. (b) Webb, S. P.; Agarwal, P. K.; Hammes-Schiffer, S. *J. Phys. Chem. B* **2000**, *104*, 8884.

(21) Alhambra, C.; Corchado, J. C.; Sánchez, M. L.; Gao, J.; Truhlar, D. G. *J. Am. Chem. Soc*. **2000**, *122*, 8197.

(22) For a review, see: Copeland, R. A.; Chan, S. I. *Ann Rev. Phys. Chem*. **1989**, *40*, 671.

(23) Wikström, *Curr. Opin. Struct. Biol*. **1998**, *8*, 480.

(24) (a) Sham, Y. Y.; Muegge, I.; Warshel, A. *Proteins: Struct., Funct., Genet*. **1999**, *36*, 484. (b) Baciou, L.; Michel, H. *Biochem*. **1995**, *34*, 7968. (c) Stowell, M. H. B.; McPhillips, T. M.; Rees, D. C.; Soltis, S. M.; Abresch, E. Feher, G. *Science*, **1997**, *276*, 812.

(25) For a recent study, see: Rastogi, V. K.; Girvin, M. E. *Nature*, **1999**, *402*, 263.

(26) Rucker, J. Klinman, J. P. *J. Am. Chem. Soc*. **1999**, *121*, 1997.

(27) Kohen, A.; Jonsson, T.; Klinman, J. P. *Biochem*. **1997**, *36*, 2603.

(28) Borgis, D.; Hynes, J. T. In *The Enzyme Catalysis Process*; Cooper, A., Houben, J., Chien, L., Eds.; Plenum: New York, 1989; p 293.

(29) (a) Antoniou, D.; Schwartz, S. D. *J. Phys. Chem. B* **2001**, *105*, 5553. (b) Caratzoulas, S.; Schwartz, S. D. *J. Chem. Phys*. **2001**, *114*, 2910. (c) Antoniou, D.; Schwartz, S. D. *Proc. Natl. Acad. Sci. U.S.A.* **1997**, *94*, 12360.

(30) Warshel, A. *Computer Modeling of Chemical Reactions in Enzymes and Solutions*; John Wiley & Sons: New York, 1991.

(31) Neria, E. and Karplus, M. *Chem. Phys. Lett*. **1997**, *267*, 23.

(32) Cui, Q.; Elstner, M.; Kaxiras, E.; Frauenheim, T.; Karplus, M. *J. Phys. Chem. B* **2001**, *105*, 569.

(33) Elstner, M.; Porezag, D.; Jungnickel, G.; Elsner, J.; Haugk, M.; Frauenheim, T.; Suhai, S.; Seifert, G. *Phys. Rev. B* **1998**, *58*, 7260.

(34) Brooks, B. R.; Bruccoleri, R. E.; Olafson, B. D.; States, D. J.; Swaminathan, S.; Karplus, M. *J. Comput. Chem*. **1983**, *4*, 187.

(35) Field, M.; Bash, P. A.; Karplus, M. *J. Comput. Chem*. **1990**, *11*, 700.

(36) Elstner, M.; Cui, Q.; Munich, P.; Kaxiras, E.; Frauenheim, T.; Karplus, M. To be submitted.

(37) Alkaradaghi, S.; Cedegrenzeppezauer, E. S.; Hovmoller, S.; Petratos, K.; Terry, H.; Wilson, K. S. *Acta Crystallogr. D* **1994**, *50*, 793.

(38) MacKerell, A. et al. *J. Phys. Chem. B,* **1998**, *102*, 3586.

(39) Stanton, R. V.; Merz, K. M. *J. Chem. Phys.* **1994**, *101*, 6658.

(40) Reuter, N.; Dejaegere, A.; Maigret, B.; Karplus, M. *J. Phys. Chem. B* **2000**, *104*, 1720.

(41) Brooks, C. L., III; Karplus, M. *J. Mol. Biol*. **1989**, *208*, 159.

(42) Simonson, T.; Archontis, G.; Karplus, M. *J. Phys. Chem. B* **1997**, *101*, 8349.

(43) Neria, E.; Fischer, S.; Karplus, M. *J. Chem. Phys*. **1996**, *105*, 1902.

(44) Archontis, G.; Simonson, T.; Moras, D.; Karplus, M. *J. Mol. Biol.* **1998,** *275*, 823.

(45) Fischer, S.; Karplus, M. *Chem. Phys. Lett*. **1992**, *194*, 252.

(46) (a) Becke, A. D. *Phys. Rev. A* **1998**, *38*, 3098. (b) Lee, C.; Yang, W.; Parr, R. G. *Phys. Rev. B* **1988**, *37*, 785. (c) Becke, A. D. *J. Chem. Phys*. **1993**, *98*, 5648.

(47) (a) Ditchfield, R.; Hehre, W. J.; Pople, J. A. *J. Chem. Phys*. **1971**, *54*, 724. (b) Hehre, W. J.; Ditchfield, R.; Pople, J. A. *J. Chem. Phys*. **1972**, *56*, 2257. (c) Hariharan, P. C.; Pople, J. A. *Theor. Chim. Acta*. **1973**, *28*, 213.

(48) Barandiaran, Z.; Seijo, L. Huzinaga, S. Klobukowski, M. *Int. J. Quantum Chem*. **1986**, *29*, 1047.

(49) Cui, Q.; Karplus, M. *J. Am. Chem. Soc.* **2001**, *123*, 2284.

(50) Bashford, D.; Cohen, F. E.; Karplus, M.; Kuntz, I. D.; Weaver, D. L. *Proteins* **1988**, *4*, 211.

(51) (a) Truhlar, D. G.; Garrett, B. C. *Acc. Chem. Res*. **1980**, *13*, 440. (b) Truhlar, D. G.; Garrett, B. C. *Annu. Rev. Phys. Chem*. **1984**, *35*, 159.

(52) Alhambra, C.; Gao, J.; Corchado, J. C.; Villà, J.; Truhlar, D. G. *J. Am. Chem. Soc*. **1999**, *121*, 2253.

(53) Cui, Q.; Karplus, M. *J. Am. Chem. Soc*. **2002**, in press.

(54) (a) Torrie, G. M.; Valleau, J. P. *J. Chem. Phys*. **1974**, *66*, 1402. (b) Allen, M. P.; Tildesley, D. J. *Computer Simulation of Liquids*; Oxford University Press: New York, 1987.

(55) (a) Ferrenberg, A. M.; Swendsen, R. H. *Phys. Rev. Lett.* **1989**, *63*, 1195. (b) Kumar, S.; Bouzida, D.; Swendsen, R. H.; Kollman, P. A.; Rosenberg, J. M. *J. Comput. Chem.* **1992**, *13*, 1011.

(56) (a) Vitkup, D.; Ringe, D.; Petsko, G. A.; Karplus, M. *Nat. Struct. Biol*. **2000**, *7*, 34. (b) Zhou, Y.; Vitkup, D.; Karplus, M. *J. Mol. Biol*. **1999**, *285*, 13471.

(57) Smith, J.; Kuczera, K.; Karplus, M. *Proc. Natl. Acad. Sci. U.S.A.* **1990**, *87*, 1601.

(58) (a) Nose, S. *J. Chem. Phys*. **1984**, *81*, 511. (b) Hoover, W. G. *Phys. Rev. A* **1985**, *31*, 1695.

(59) For a recent review, see: Thiel, W. *Adv. Chem. Phys*. **1996**, *93*.

(60) (a) Decornez, H.; Drukker, K.; Hammes-Schiffer, S. *J. Phys. Chem*. **1999**, *103*, 2891. (b) Decornez, H.; Hammes-Schiffer, S. *Isr. J. Chem*. **1999**, *39*, 397

(61) These barriers were estimated from the rate-constants measured from ref 8 on the basis of a transition-state theory: i.e., $k = k_B T/h \exp(-\Delta G^{\neq}/k_B T)$, where $\Delta G^{\neq}$ is the activation free energy. A prefactor of $k_B T/h$

was assumed, which was found to be appropriate in our previous kinetic modeling of triosephosphate isomerase (ref 49).

(62) Dworschack, R. T.; Plapp, B. V. *Biochem*. **1977**, *16*, 2716.

(63) Dalziel, K. *J. Biol. Chem*. **1963**, *238*, 2850.

(64) (a) Bashford, D.; Karplus, M. *Biochem*. **1990**, *29*, 10219. (b) Bashford, D.; Karplus, D. *J. Phys. Chem*. **1991**, *95*, 9556.

(65) Beroza, P.; Fredkin, D. R.; Okamura, M. Y.; Feher, G. *Proc. Natl. Acad. Sci. U.S.A.* **1991**, *88*, 5804.

(66) Ganzhorn, A. J.; Plapp, B. V. *J. Biol. Chem*. **1988**, *263*, 5446.

(67) Ryu, J. W.; Lee, K. M. *Arch. Pharm. Res*. **1997**, *20*, 115.

(68) Tsai, S.; Klinman, J. P. *Biochem*. **2001**, *40*, 2303.

(69) In the current work, a "classical" description means that no tunneling along the reaction coordinate is considered although zero-point energies in the bound vibrational modes are included; i.e., this is equivalent to the "semiclassical" limit referred to in experimental literature (e.g., ref 22) Here, "semiclassical" is reserved for the WKB-based treatment of tunneling.

(70) For example, see: (a) Truong, T. N.; McCammon, J. A. *J. Am. Chem. Soc*. **1991**, *113*, 7504. (b) Storer J. W.; Houk, K. N. *J. Am. Chem. Soc*. **1993**, *115*, 10426.

(71) Huskey, W. P. *J. Phys. Org. Chem*. **1991**, *4*, 361.

(72) Bigeleisen, J. *J. Chem. Phys.* **1955**, *23*, 2264.

(73) Cha, Y.; Murray, C. J. Klinman, J. P. *Science* **1989**, *243*, 1325.

(74) Bell, R. P. *The Tunnel Effect in Chemistry*; Chapman and Hall: London, 1980.

(75) For a recent review, see: (a) Talkener, P., Häggi, P., Eds. *New Trends in Kramers' Reaction Rate Theory*; Kluwer Academic: Dordrecht, 1995. (b) Hänggi, P., Pollak, E., Grabert, H., Eds .*The Quantum Kramers Problem*; University of Augsburg: Augsberg, FRG, 1989.

(76) Karplus, M. *J. Phys. Chem. B* **2000**, *104*, 11.

(77) (a) Berezhkovskii, A. M.; Szabo, A.; Weiss, G. H.; Zhou, H.-X. *J. Chem. Phys.* **1999**, *111*, 9952. (b) Doering, C. R.; Gadoua, J. C. *Phys. Rev. Lett*. **1992**, *69*, 2318.

(78) Agmon, N.; Hopfield, J. J. *J. Chem. Phys*. **1983**, *79*, 2042.

(79) (a) Lu, H. P.; Xie, X. S. *J. Biol. Chem.* **1999**, *274*, 15967. (b) Lu, H. P.; Xun, L. Y.; Xie, S. *Science*, **1998**, *282*, 1877. (c) Edman, L.; Foldes-Papp, Z.; Wennmalm, S.; Rigler, R. *Chem. Phys*. **1999**, *247*, 11.

(80) Petrich, J. W.; Lambry, J.-C.; Kuczera, K.; Karplus, M.; Poyart, C.; Martin, J.-L. *Biochem.* **1991**, *30*, 3975.

(81) Neria, E.; Karplus, M. *J. Chem. Phys*. **1996**, *105*, 10812.

(82) Bruice, T. C.; Benkovic, S. J. *Biochem*. **2000**, *39*, 6267.

(83) Yang, L.; Post, C. *Biochem*. **1996**, *48*, 15129.

(84) Bash, P. A.; Field, M. J.; Davenport, R. C.; Petsko, G. A.; Ringe, D.; Karplus, M. *Biochem.* **1991**, *30*, 5826.

(85) Zavodszky, P.; Kardos, J.; Svingor, A.; Petsko, G. A. *Proc. Natl. Acad. Sci. U.S.A.*, **1998**, *95*, 7406.

(86) For an interesting discussion, see: Truhlar, D. G., Kohen, A. *Proc. Natl. Acad. Sci. U.S.A.*, **2001**, *98*, 848.

(87) For example, see: Miller, W. H. *J. Phys. Chem.* A **2001**, *105*, 2942.